Motion Planner for Skid-Steer Unmanned Ground Vehicle

MAIDO HIIEMAA

TALLINN UNIVERSITY OF TECHNOLOGY
Faculty of Mechanical Engineering
Department of Mechatronics

Dissertation was accepted for the defence of the degree of Doctor of Philosophy in Engineering on July 8, 2013.

Supervisor: Prof. Mart Tamre, Department of Mechatronics,
Tallinn University of Technology, Estonia

Opponents: Professor Janis Viba, Faculty of Transport and Mechanical Engineering,
Riga Technical University, Latvia

Professor Jari Juhanko, Department of Engineering Design and Production,
Aalto University, Finland

Defence of the thesis: August 26th 2013 at 11:00
Tallinn University of Technology
Ehitajate tee 5, Tallinn, Estonia

Declaration:
Hereby I declare that this doctoral thesis, my original investigation and achievement, submitted for the doctoral degree at Tallinn University of Technology has not been submitted for any academic degree.

/Maido Hiiemaa/

European Union
European Social Fund   Investing in your future

Liikumise plaanija külisroolimisega mehitamata maasõidukile

MAIDO HIIEMAA

CONTENTS

LIST OF PUBLICATIONS

1. Hiiemaa, M., Tamre, M. Low speed motion feedback for the unmanned ground vehicle. /ed. T. Otto — *Proc.of the 8th International Conf. of DAAAM Baltic, Industrial Engineering*. 2012, I, 293–300

2. Hiiemaa, M., Tamre, M. Assisting Control Algorithms for Simplified Operation of Remotely Controlled Unmanned Ground Vehicle. /eds. I. Skiedraite, J. Baskutiene, E. Dragašius — *Mechatronic Systems and Materials (MSM 2011) 7th International Conference*. Kaunas : Kaunas University of Technology Press, 2011, 1–5

3. Hiiemaa, M., Tamre, M. Semi-autonomous Motion Control Layer for UGV-Type Robot. /eds. T. Brezina, R. Jablonski — *Recent Advances in Mechatronics 2008-2009*. Springer, 2010, 203–207

4. Hiiemaa, M., Tamre, M. Intelligent Energy Management of Unmanned Ground Vehicle. /ed. R. Küttner — *7th International Conference of DAAAM Baltic Industrial Engineering*. Tallinn : Tallinn University of Technology Press, 2010, 542–547

INTRODUCTION

Employment of Unmanned Ground Vehicles (UGVs) in military and civil applications shows a clear tendency of growth. Rapid development of UGVs allows performing an increasing amount of tasks with an assistance of remotely controlled mobile robots. UGVs are often used to avoid human contact with Improvised Explosive Devices (IEDs), fire, toxic gases and radiation. Despite its simplicity, the 4-wheel skid-steer type UGV concept is still widely studied [1–9] and used [10–18]. Its high maneuverability and simple design, compared to explicit steering, often make this undercarriage type the concept of choice in a wide range of applications, as seen in Figure 1a-c.

(a)   *(b)*   *(c)*
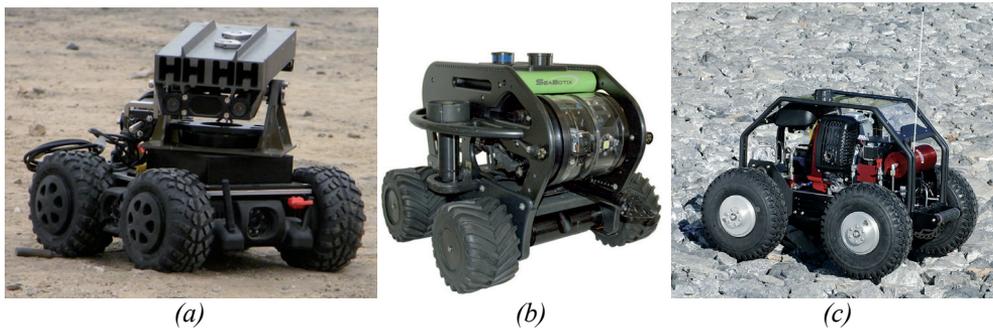
Figure 1. UGVs for various applications: (a) counter-IED system – Pincher UGV [11]; *(b) underwater mobile robot – Little Benthic Crawler* [10]; *(c) all-terrain gas-powered UGV for experimenting with tire physics – Parallax QuadRover* [18]

Some of the UGV applications have special requirements for the UGV motion in order not to damage extremely delicate on-board instrumentation. Limited motion parameters are often required when handling and transporting potentially live IEDs, antennas, high-end camera systems etc. Keeping motion parameters of UGVs within safe limits often relies on the skillfulness of the UGV operator who is handling the controls of the Control Station.

One unique 4-wheeled skid-steer UGV was developed and built in TUT Department of Mechatronics [19] by a small team (where the author of this thesis developed mostly on-board control) for a wide range of applications. It has a capability to increase its clearance by repositioning its legs. High clearance mode makes zero-radius turning energy efficient but elevated center of weight and UGV suspension cause the UGV to rock at sudden and intense deceleration. Outdoor experiments with this UGV showed that unprocessed user input is not very suitable for controlling such vehicles. UGV operator is prone to overreact to the potential threats and even make things worse with too intense braking, possibly flipping the vehicle over. The initiative to start developing methods and algorithms for effortless and safe driving for 4-wheel skid-steer vehicles originated from the practical needs of this project.

Figure 2. Universal UGV developed and built in TUT Department of Mechatronics [19]

UGV missions may have different sections of path or tasks with different motion control requirements. For example, driving hundreds of meters to an IED may be performed at maximum velocity, jerk and acceleration limits but the last few meters of the approach insist on proper reduction of these limits. After the IED pickup, another set of motion parameter limits could be recalled from memory. Changing the motion parameter limits according to the nature of planned tasks is task-specific and must be made by the UGV operator. Once critical motion parameter limits have been chosen, UGV control algorithms should keep motion parameters of the UGV from violating those limits, so the UGV operator can concentrate mostly on controlling the UGV by velocity and turning radius.

Motion planner methods are necessary to make safety-critical skid-steer UGV control effortless to the UGV operator. Other benefits of using motion planning control modules between user input and low level motion control modules, which perform the prescribed motion, are increased energy-efficiency and less tear and wear to the UGV wheel actuators.

Main objectives of the thesis

- To develop a method for the UGV control with impact reduction to the UGV system and safety-critical loading
- To develop a method for use in the UGV control keeping critical motion parameters of the UGV limited yet allowing maximum controllability by the user input
- To create virtual models for testing the proposed concepts by computer simulations

Algorithms and models for the UGV control should be made as simple as possible to allow later extensions to the software without high performance requirements when implemented as a real-time system.

Structure of the thesis

Review of the literature in Chapter 1 in this thesis is by no means exhaustive. It serves as a linkage between the current study and other studies about similar control problems. Numerous investigations and growing usage of unmanned 4-wheel skid-steer vehicles prove the necessity of research and development of related technologies. Abstract control system descriptions use general approaches from modern robotic literature and add necessary details in later chapters.

Basically, the structure of the thesis is composed of the step-by-step additions to the initially presented concepts as new shortcomings of the concepts have been identified. In many cases, the extended functionality of control modules can be altered according to the need for specific simulations and comparisons.

Straight driving mode on a horizontal flat terrain is discussed in Chapter 2. In this mode AMPP (Active Motion Profile Planner) modules keep tangential jerk, acceleration and velocity within their task-specific limits. Part of motion and path planning software handles halting the vehicle safely at the automatic stopping point. This functionality simplifies docking with the docking station and halting the vehicle smoothly before colliding with obstacles. Small adjustments are possible to shorten the distance of a predicted full stop point without increasing the limits of motion parameters. Emergency stopping scenario requires overriding default set of motion parameter limits.

Chapter 3 analyzes a possibility to use AMPP modules for controlling tangential motion of the left and right side reference point of the UGV. Shortcomings of using this method have been also presented.

Chapter 4 provides a solution for keeping the maximum acceleration magnitude within safe limits. Certain velocity combinations must be excluded from the command space by reducing the proportional velocity command to make turning at full velocity safe. Another command processing method is proposed to avoid one possible exception where the maximum acceleration magnitude could violate its limit. Turn by braking makes the UGV control more consistent at higher velocities. Simulations results have proven the efficiency of the methods. At the end of this chapter, detailed charts are given about the data flow between proposed control modules and guidelines for selecting motion parameter limits are provided.

In Chapter 5 the proposed methods are evaluated to be used in trajectory planning. Further development of tentacles method would be useful in reference path tracking, evaluation and optimization, connecting this topic to the ideas from other studies presented in the section of Future work.

ABBREVIATIONS AND SYMBOLS

4WD	Four-Wheel Drive
AMPP	Active Motion Profile Planner
CA	Critical Area
CNC	Computer Numerical Control
COR	Center Of (turning) Radius
CPP	Command Pre-Processor
CPU	Central Processing Unit
FFB	Force Feed-Back
IED	Improvised Explosive Device
IMU	Inertial Measurement Unit
MP	Motion Planner
PVCR	Proportional Velocity Command Reduction
REED	Reverse Exponential Error Decay
STRA	Small Turning Radius Avoidance
TBB	Turn By Braking
UGV	Unmanned Ground Vehicle

θ	orientation of the UGV frame (chassis)
ω	angular velocity of the UGV frame
α	angular acceleration of the UGV frame
β	angular jerk of the UGV frame
a	tangential acceleration (left or right side)
a_L, a_R	tangential acceleration of the left and right reference point
a_{lim}	tangential acceleration limit of a reference point
a_{limit}	maximum acceleration magnitude allowed in the CA
a_{max}	maximum magnitude acceleration within the CA
a_n	acceleration command for next interval
a_r	radial acceleration
a_t	tangential acceleration
a_{tar}	target acceleration
a_x, a_y	gravitational acceleration along the x and y-axis
b	velocity reduction coefficient
c_1	distance between the minimum magnitude point of the total acceleration field and the convergence point of the converging vector field
c_2	distance between the minimum magnitude point of the total acceleration field and the circulation point of the solenoidal vector field
d	distance from the farthest point within the CA to the center of the total acceleration vector field

i	variable for counting simulation cycles
j	tangential jerk (left or right side)
j_L, j_R	tangential jerk of the left and right reference point
j_{lim}	tangential jerk limit of a reference point
j_n	jerk command for the next interval
l	track width of the UGV and distance between reference points
l_1	distance 1 m
r_ω	distance from the center of angular velocity
r_α	distance from the center of angular acceleration
r_{COR}	displacement of COR (to the left of UGV)
r_{CORa}	displacement of tangential acceleration vector field center
r_{CORj}	displacement of tangential jerk vector field center
s	distance (along the path of a reference point)
s_C	distance command (same as distance limit)
s_{lim}	distance limit (automatic halting point)
t	time
t_{mc}	time-step duration
v	tangential velocity (left or right side)
v_C	velocity command
v_{dec}	velocity change by the time acceleration reaches zero
v_L, v_R	tangential velocity of the left and right reference point
v_{lim}	tangential velocity limit of a reference point
v_{max}	maximum velocity command from user input
v_{tar}	target velocity
v_{tol}	target velocity tolerance
x_1, y_1	offset of total acceleration vector field center along the x and y-axis
x_2, y_2	additional shifting of the acceleration vector field's minimum magnitude point along the x and y-axis

1. REVIEW OF THE LITERATURE

1.1 Robotic architectures

Robotic architectures can be divided into two main concepts: function-based and behavior-based. Motion planning is used only in function-based robotic architectures (Figure 3). Many robotic functions are planned in advance for the task-oriented systems. Thus, the 'plan' represents a planner, normally an algorithm residing in the on-board computer [20]. The complexity of motion planning algorithms may prove to be too burdensome for real-time operation. In applications which are similar to CNC router programming the environment is usually static enough to calculate motion planning of the entire routing program before the motion of the tool is initiated. Even if UGVs were used in a fully mapped static environment, the motion of the UGV could not be fully predicted. Even small variations of tire grip cause skid-steer UGVs to increasingly deviate from initially planned motion scenarios.
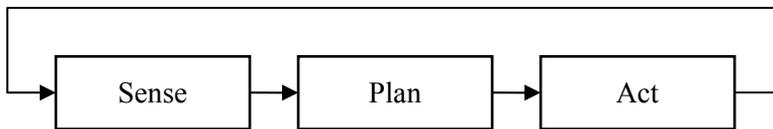
Figure 3. *Function-based robotic architecture paradigm* [21]

Behavior-based robotic architecture (Figure 4) is suitable for fast and simple system responses. Using only behavior-based robotic architecture alone does not satisfy the requirements of partial predictability and planning in the UGV control. It is, however, possible to use it in low level motion control layers.
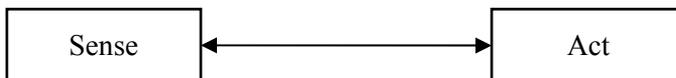
Figure 4. Behavior-based robotic architecture paradigm [21]

Comparison of conventional robotic architectures is shown in Table 1. Both architectures have some critical aspects, which are required for the UGV control. The main drawback of function-based architecture is a slow response due to a heavy computational burden. Having any kind of motion planning would make it possible for UGV control modules to prevent unforeseen collisions, which would otherwise occur due to human error.

Table 1. *Features of Robotic Architectures* [20]

Function-Based/Deliberative Architecture	Behavior-Based/Reactive Architecture
Planning is required/planner based	No planning is required
Heavy computational burden	Lower computational burden
Has slow response	Has fast response
World representation is required and used	No world representation is used
Suitable for static environment	More suitable for dynamic environment
Relatively high level of intelligence is used	Relatively low level of intelligence is used

Layered approach helps to create insightful hierarchy between control modules with different nature based on functionality, connections and levels of abstraction. There is no fixed limit to the number of layers, but three-layered architecture has become very common in robot control architectures [20]. Top layer is deliberative, middle layer is reactive and lower level controls sensors and actuators (Figure 5).

Functional
layer

Behaviour
layer

Control
layer

Environment
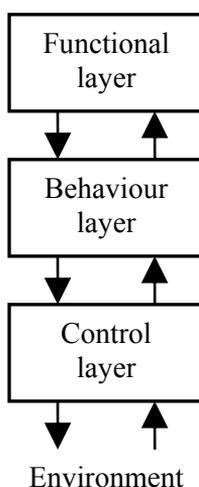
Figure 5. A three-layered robotic architecture [20]

1.2 Motion profile planning

In this thesis, motion analysis is often illustrated by the motion simulation plots with a time-step of 10^{-2} s. This interval has been chosen for the time axis because it is also the main cycle interval of the UGV control algorithms, which are used for testing and evaluating the proposed methods in later sections of the thesis.

Optimal main cycle interval for UGV on-board software is dependant on the actual UGV hardware specifics and motion characteristics. At ultra low velocities the simple pulse counting method should be replaced with more advanced methods [22–25] with additional custom hardware. The effectiveness of using such methods, however, relies heavily on the low (random) noise of the wheel encoders and, in most cases, on the lack of mechanical imperfections of the encoder.

Jerk, the third derivative of position, plays an important role in servo motion control. Having a large jerk may cause vibrations, excitations of not modeled dynamics and high wear to the mechanical parts [22–24]. High jerk peaks, therefore, may harm delicate on-board equipment as well. Another study shows that minimum energy is in comparable agreement with the minimum jerk [25]. Lowered energy consumption is undoubtedly a very desirable feature for UGVs, which operate on batteries for long periods of time. In [26] shaping of torque was used for reducing jerk. This thesis starts from limited jerk pulses to create all other parameters of motion.

To make a UGV platform move from one position to another, starting from a steady state and ending with a steady state, within a shortest possible time span, while also keeping jerk strictly limited, the fastest possible motion profile is determined by the jerk (upper and lower) limits (illustrated in Figure 6). Only four states (T_0 to T_3) are necessary (where T_0 is idle state) for that type of motion profiles. This type of motion profile can be used only for moving short distances at acceleration, because acceleration and velocity quickly become non-performable by the machinery.
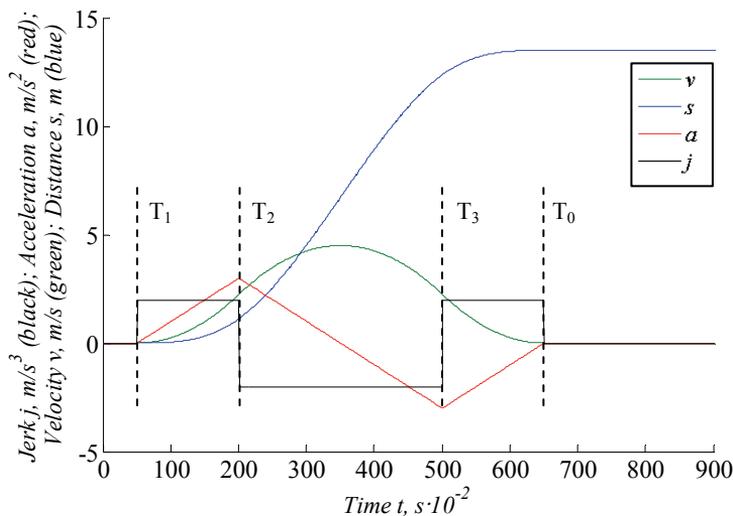
Figure 6. Simple third order motion profile with limited jerk

In this example, jerk assumes values j_{lim} and $-j_{lim}$ at the driving state and zero jerk before and after the movement. Any other values of jerk would either waste time or violate the symmetric jerk limits $[-j_{lim}, j_{lim}]$. Creating motion profiles for CNC machines where jerk has only three possible levels to avoid impact on the motors was used in [27].

Because there is usually a need for limited jerk, acceleration and velocity, the entire motion profile must consist of more distinguishable sections and the timing of jerk pulses is more complicated. In CNC systems where position limit is also used, there are seven active stages (T_1 to T_7) of motion used [28], T_0 being the idle

15

state. All active states are not required in some motion scenarios. Accurate timing of jerk pulses makes it possible to satisfy acceleration, velocity and distance limits without the need for oscillating jerk, as shown in Figure 7.
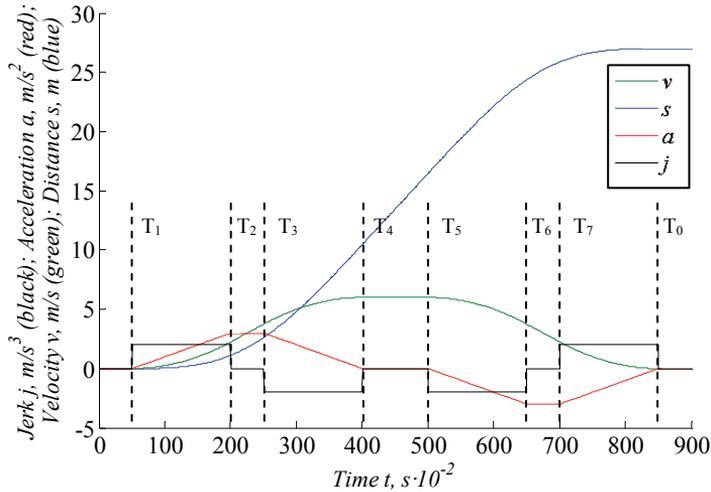
Figure 7. Timing of jerk pulses to keep other motion parameters limited

Weak points of ideal motion profiles are: limited time resolution for jerk pulses and virtually no spare time for adjustments when unpredicted positive disturbance (increasing the velocity) or shortening the distance to the automatic halting point occurs, which neglects the other motion parameter limits of safe motion profile. Negative unpredicted disturbance before the planned halting point would simply cause a motion planner to create new motion profiles and cause no overshoot. Low resolution wheel encoders necessitate using long time-steps if the pulse counting method is used. Mere timing of jerk signal pulses, therefore, is not suitable for the UGV motion control.

Scientific literature about the critical motion of the frame of skid-steer UGVs is scarce. To keep the motion parameters of the UGV frame and delicate on-board equipment limited it is required to investigate the problems and develop suitable methods and algorithms for specific UGV control with limited critical motion parameters.

Ideal motion profiles (S-curve velocity profiles) have often symmetric velocity curvatures at accelerating and decelerating, as seen in Figure 7. Asymmetric S-curve motion profile is sometimes used for more flexibility in managing the jerk values and to have smoother arrival to the target position [29].

Another work [30] proposes an alternate method to a conventional S-curve velocity profile. It has unique jerk pulse shaping to reduce residual vibration of the machinery.

1.3 Motion planning

Early research of motion planning mainly focused on industrial robot systems, and later extended to the mobile robots [31]. The terms "motion planning" and "trajectory planning" are often used in robotics to describe the functionality of algorithms that convert high-level specifications of tasks from humans into low-level descriptions of how to move [32].

Choosing between virtual tentacles (alternative paths which a mobile robot can track) is a very intuitive method for using it in local path planning and obstacle avoidance. Shape of the tentacles can be made according to the capabilities of a particular mobile robot. Tentacles that are close to obstacles can be automatically excluded from the selection.

Circular-arc virtual tentacles proposed in [33] are not very suitable for skid-steer UGV, with a requirement for jerk reduction, because instantaneous turning radius change contributes to the instantaneous centripetal acceleration change.

Another study focuses on the selection of tentacles, considering also reference path [31]. Tentacle-based approach has been used also along with visual navigation by the on-board actuated camera [34].

1.4 Chapter summary

- Recent literature about the relevant topics of robotics was reviewed in this section of the thesis.
- Conventional function-based robotic architecture paradigm addresses motion planning, but may not guarantee the best possible response for UGV control when sophisticated planning methods are used. Conventional behavior-based robotic architecture paradigm does not use motion planning, which would be a requirement for safe and partially predictable UGV control.
- Layered approach helps to create insightful hierarchy between control modules with different nature based on functionality, connections and levels of abstraction.
- Jerk must be kept within limits and acceleration must be kept continuous to prevent impact on servos and the CA of the UGV.
- Accurately set time gaps between jerk pulses make it possible to indirectly control other motion parameters and keep other motion parameters limited.
- Using ideal motion profiles for UGV control has an important limitation when the automatic stopping point is brought closer to the UGV.
- Reports on controlling skid-steer vehicles are scarce, thus it is difficult to propose methods for keeping UGV motion safe for a UGV system and loading.

2. MOTION PLANNING FOR STRAIGHT MOTION

2.1 Reference points and the Critical Area of the UGV

The dashed circle in Figure 8 describes the perimeter of a certain area where delicate equipment should be placed. It is named CA (Critical Area). This area may be resized according to the needs to install delicate on-board equipment, but it is always concentric with the center of UGV. UGV Control algorithms regard only motion of the UGV frame and equipment within this circular area.
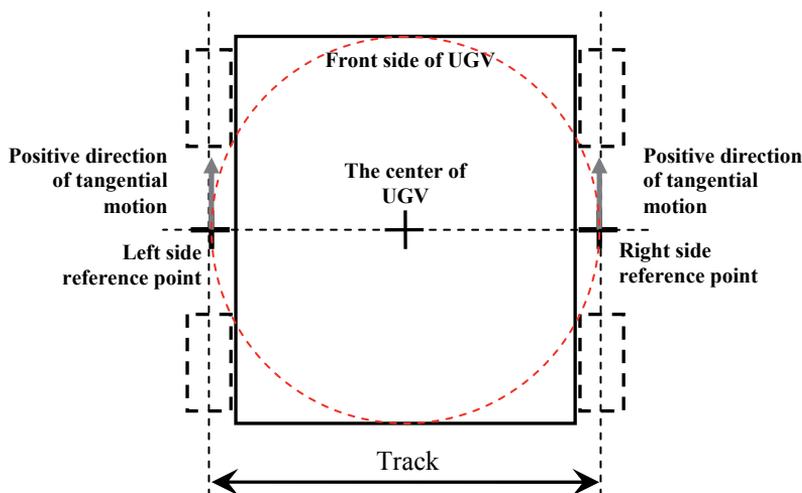
Figure 8. UGV Frame with reference points and the Critical Area

Two reference points (left side reference point and right side reference point) are used to define and analyze the motion of the UGV frame by the tangential and radial acceleration components of these points. In straight motion on a level and flat terrain, due to the lack of centripetal and gravitational acceleration components, only tangential components are present. Straight motion analysis considers only identical tangential motion of the left and right reference point of a UGV.

2.2 Layered approach in the skid-steering UGV control

Figure 9 shows the layers of the UGV control presented hierarchically with main data flow connections. User input may be replaced with an additional higher level, control layers for more autonomous control. The higher layer of the MP (Motion Planner) is the CPP (Command Pre-Processor). This layer alters or excludes unsafe combinations of velocity commands to keep maximum acceleration magnitude from exceeding its prescribed limit in any part of the UGV CA.

Left and right side AMPP (Active Motion Profile Planner) modules handle tangential motion of the left and right side reference points of the UGV.
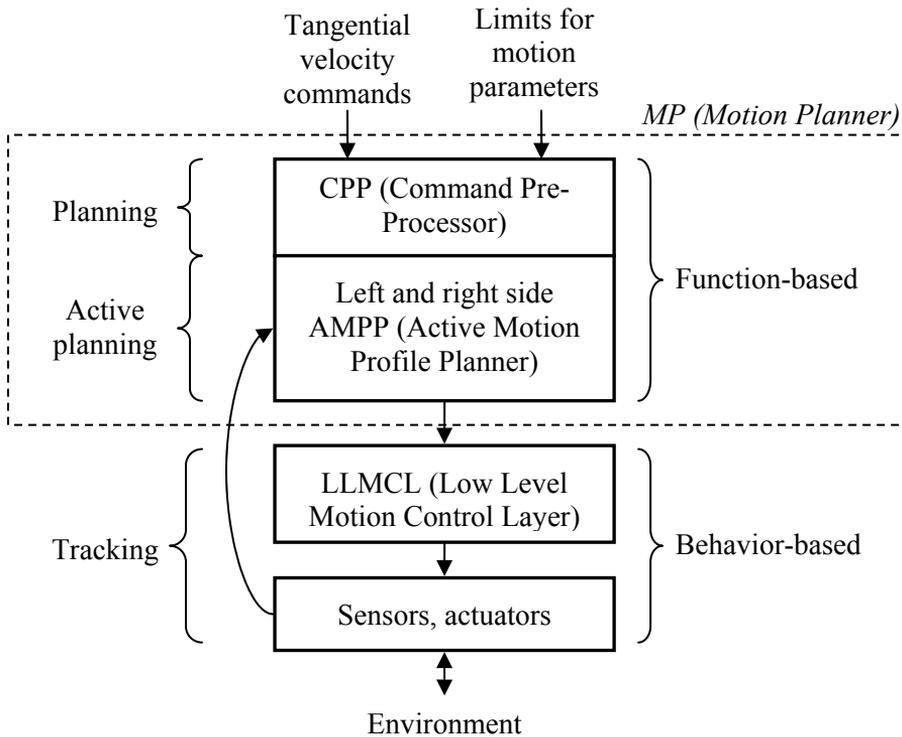
Figure 9. Layered approach of the UGV control

Low Level Motion Control Layer is a feed-forward type UGV and a terrain-specific module to make UGV motion less distorted by the known disturbances. To develop this layer real life experiments with actual UGV are required and its performance is highly dependant on many uncertain characteristics of the terrain. Motion of the UGV frame and wheels is fed back to AMPP modules to create the best possible motion scenarios for every situation. Deviation from simulated motion scenarios is overcome by iterative algorithms that take real measurements as input.

Disturbance rejection and approximation noise in low velocities have been discussed in earlier publications of the author. This layered approach transfers these functionalities to Low Level Motion Control Layer (LLMCL), which is not studied in this thesis. Current work focuses on kinematics of skid-steer type UGVs and proposes methods on control to avoid unsafe motion of the CA.

2.3 Active Motion Profile Planner

AMPP is a motion profile planner to control tangential motion of either left or right side reference point of the UGV. For symmetrical motion, one AMPP module can control both sides in parallel. In most parts of the thesis, the following (default) set of limits (Table 2) is used for concept demonstrations.

Table 2. Default motion parameter limits for AMPP

Parameter	Symbol	Maximum value	Minimum value
Jerk, m/s^3	j_{lim}	2.5	−2.5
Acceleration, m/s^2	a_{lim}	3.0	−3.0
Velocity, m/s	v_{lim}	2.0	−2.0

Motion parameter limits have been chosen symmetric to zero, because instrumentation within the CA has equal sensitivity to motion from both directions.

Jerk level 4 m/s^3 was considered suitable for elevator control in [35] for the comfort of passengers. When designing a train and elevators, engineers will typically be required to keep the jerk less than 2 m/s^3 for passenger comfort [36]. Tangential jerk of 2.5 m/s^3 was chosen as default jerk limit for most concept testing of proposed methods in this thesis.

Acceleration limit was chosen 3.0 m/s^2, which is roughly a third of gravitational acceleration.

Velocity limit 2.0 m/s was chosen close to the maximum velocity of the UGV built it TUT [19].

Distance limit has no default value. It is set and continuously updated when the UGV sensors detect an obstacle or the UGV drives to a docking station.

In the literature [29, 27, 24], it is common to use analytical methods for describing the behavior of the system during different system states. AMPP software uses numeric simulation models to find the best fitting timing for jerk pulses. Numeric simulation models can be easily tested with data acquired from actual vehicles that are driving along certain paths. Also, switching between mathematical functions, which a motion planner uses, can be made effortlessly.

Because in real-time operation, user input and the environment of the UGV may change arbitrarily, the final motion scenario cannot be determined in advance. Still, there are parts of the motion scenario which can do it. For example, knowing all the limits of motion parameters, laws for scenario-creation and actual motion parameters, a full halt scenario with an optimal time can be simulated at any time-step of the UGV control. Knowing the time and distance requirements of the normal stopping scenario in advance allows control software to trigger intensified or emergency stopping mode if needed. An AMPP uses only a few simple short-term simulations, each time-step, to find the most suitable output command for the UGV control. The actual motion profile is being created time-step by time-step as more recent data arrives from sensors.

REED (Reverse Exponential Error Decay) motion profile planning mode combines fast response on the first phases of motion, with smooth settling in phases where fast response is not required. By changing the jerk and acceleration limit, it is possible to prolong or shorten the duration of the fast response phase. By using the default tangential motion parameter limits, the duration of jerk trimming (jerk saturation) is short, as seen in Figure 10.
Jerk command is calculated by a simple formula:

$$j_n = \frac{a_{tar} - a}{100t_{mc}}, \tag{1}$$

where j_n – jerk command (for next interval); a_{tar} – acceleration target (can only have values a_{lim}, $-a_{lim}$ or zero); a – actual acceleration of the vehicle at current stage; t_{mc} – main cycle interval.

Coefficient 100 is used for normalizing the formula. Before trimming the jerk command, the function represents almost perfectly reverse natural exponential function (e^{-x}) in the time domain. Insignificant distortion is introduced by the usage of numeric simulation being performed in discrete time.

Acceleration for the next (adjacent) time-step is calculated by the formula:

$$a_n = a + j_n t_{mc}, \tag{2}$$

where a_n – acceleration command for the next time-step.

Here and in several further simulations jerk is trimmed in software to the closest permitted level, whenever it violates default jerk limit.

Distance limit for normal drive conditions is large enough not to cause velocity suppression due to the proximity of the limit. Automatic halt sequence can be started manually or automatically by setting the distance limit close to the UGV.

Figure 10 illustrates how an AMPP, which uses mostly the REED planning mode, generates fast response at the beginning of the movement and allows fine adjustments of motion parameters when fast response is not required.
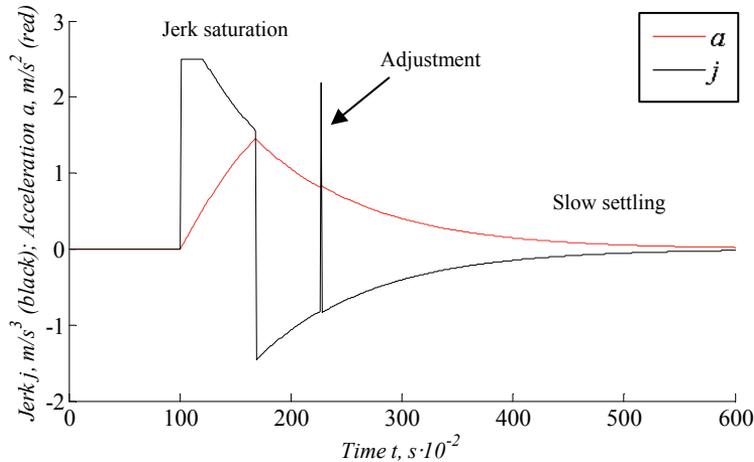
Figure 10. Demonstration of motion planner jerk saturation

In case the automatic halt point needs to be slightly corrected, just before the vehicle has come to a complete standstill, the system has still a fair amount of controllability because the jerk command is not saturated as in an ideal mode.

Figure 10 also demonstrates how a short jerk peak (occurring about 230 ms from the start) adjusts a UGV motion scenario to reach target parameters more accurately. This particular jerk peak was introduced by the control algorithm to reach target velocity more accurately. Jerk peaks occur more frequently, when the velocity command and/or distance limits are changed, while the UGV is in motion. Most of the simulations in this work represent a jerk to resemble a natural decay, which is trimmed according to the jerk limit in control algorithms.

Using default limits of motion parameters and **identical** velocity command sequences as input, two motion scenarios were created to demonstrate the differences between two motion profile planning modes (Figure 11 and 12).
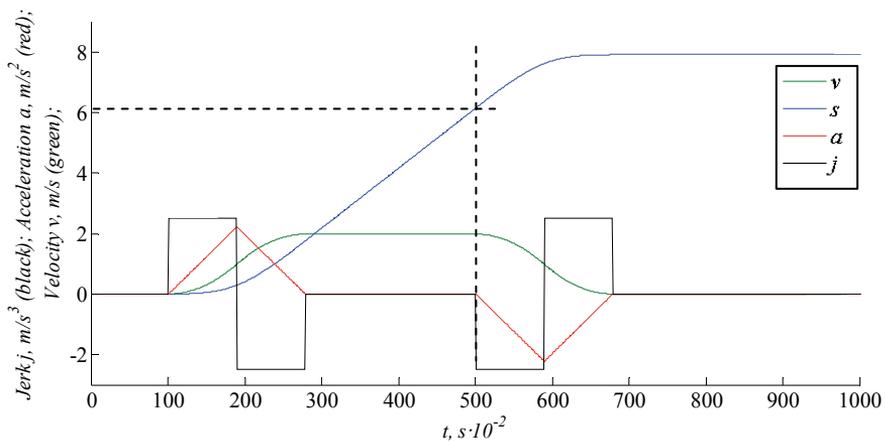
Figure 11. Motion profile planner working in an ideal mode
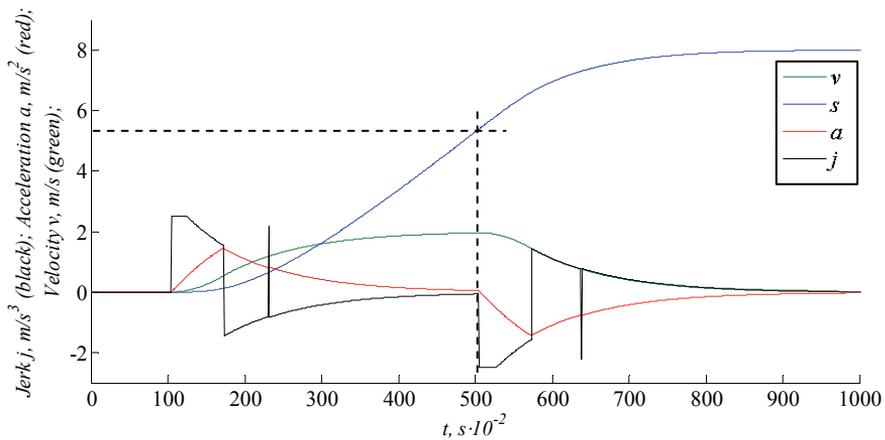
Figure 12. Motion profile planner working mostly in the REED mode

22

Despite the very different curvatures of actual motion parameters, in both motion scenarios the UGV moves a total of 8 m.

In the ideal motion planning mode, the halt scenario from full velocity (2 m/s) to a standstill requires about 1.8 m. The REED motion planning mode requires about 2.7 m. Because of obvious difference in the full halt distance, switching to the ideal mode can be used for collision avoidance as a first resort instead of changing the default limits of motion parameters.

Using asymmetric velocity curvatures, as in the REED method, for motion profile planning has an advantage when the automatic stopping point was to be misplaced a bit too far. The resulting collision would occur at much lower velocity than in the ideal mode, as seen by the velocity curvatures in Figure 11 and 12. Arrival to the target position has been made deliberately slow also in [29] by using motion profiles of the asymmetric velocity curve.

Practical results of this work [30] suggest that a smoothly decaying jerk of REED motion profile planning reduces residual vibrations (rocking) of the UGV as well when it is halted.

For AMPP to work without problems, a system of priorities must be set among motion commands. Regardless of the hierarchy of priorities, lower priority motion parameters still must follow certain rules.

Distance has the highest priority. As soon as short-term simulation of a full halt scenario predicts a halt distance, which matches the distance to the automatic stopping point or is shorter, the velocity command will be overridden by the target velocity of zero. If the automatic halting point or the obstacle moves farther from the UGV and the halt distance is too short, AMPP disables the velocity override until the halt distance becomes suitable again for a stopping scenario. The duration of the full halt scenario depends on the chosen set of limits of motion parameters and initial motion parameters. For example, it takes about 5 seconds for the UGV to come to full standstill from the initial velocity of 2 m/s, provided the default set of motion parameter limits is used. Short-term simulations have to be long enough to simulate the halt scenario up to the simulated standstill of the UGV.

If the automatic halt point is set at the opposite side of the UGV direction of motion, the UGV halt scenario is initiated by setting the target velocity to zero. Reversing of the UGV is not made automatically. Only when the UGV operator changes the sign of the velocity command, the motion to the automatic stopping point will be completed. This fail-safe helps to prevent unintentional UGV reversing due to a faulty obstacle sensor or badly chosen automatic stopping point.

Similar behavior where the UGV misses the automatic stopping point because of the limits of motion parameters is shown in Figure 13a-c. In this illustration the stopping point is set towards the movement of the UGV but the UGV is unable to stop at this point. After the vehicle has stopped, it cannot start moving in conflict with the velocity command sent from the Control Station.

Vel. ⟶
Vel. cmd. ⟶

↑   ↑
Automatic   Closest possible
stopping point   stopping point

(a)

Vel. (zero)
Vel. cmd. ⟶

↑   ↑
Automatic
stopping point

(b)

Vel. (increasing) ◄
Vel. cmd. ◄

↑   ↑
Automatic
stopping point

(c)
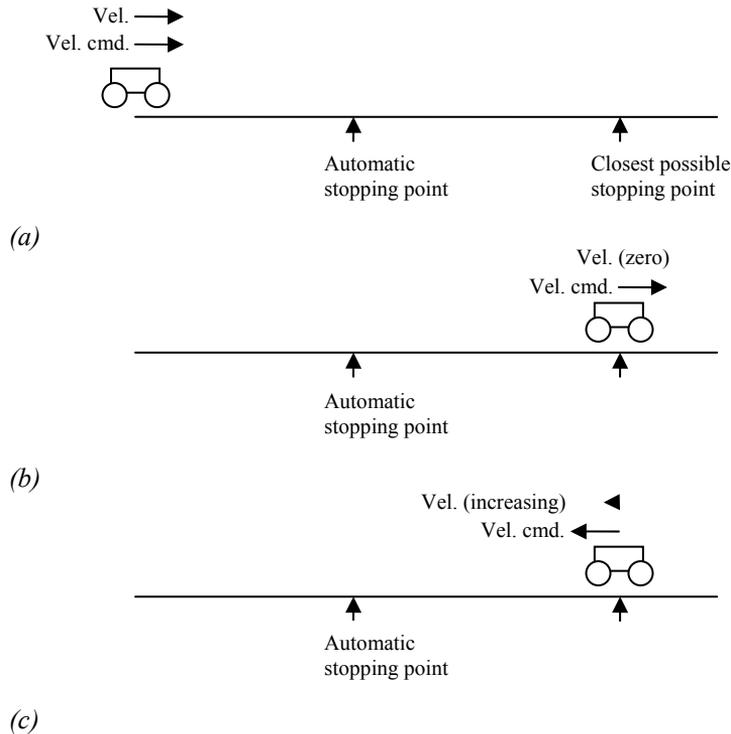
Figure 13. Automatic stopping fail-safe: (a) stopping scenario in progress; (b) waiting for velocity command change; (c) start reversing to stop at the automatic stopping point

At normal drive (without the need for setting a distance limit), every time the UGV operator changes the direction of the UGV tangential velocity, the automatic stopping point should be set to a proper side of the UGV even if the distance to it is unreachably far. To avoid sending redundant information while using only normal drive mode, the automatic stopping functionality could be disabled. In Simulink software, the automatic stopping point functionality is rarely used and has not been fully implemented.

Velocity has a lower priority. At every time-step, AMPP predicts the scenario of acceleration decay from the current value to zero, and finds the potential velocity change. Depending on the difference between the velocity command and the actual velocity added to the potential (unavoidable) velocity increase, AMPP switches to the appropriate target acceleration.

Acceleration has even lower priority. It depends on the acceleration target (which may have three discrete values). Switching between those values is made when the predicted velocity change becomes sufficient.

Jerk has the lowest priority. It is trimmed by the upper and lower jerk limit. Additionally, a jerk is gradually suppressed as acceleration nears its asymptotic (target acceleration) value.
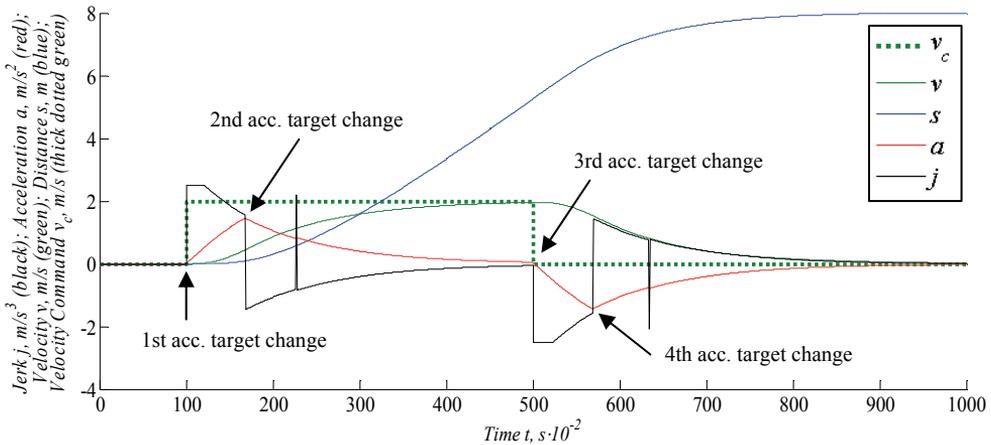
Figure 14. Full scenario of UGV driving from one point to another

End of Figure 14 demonstrates similarity of decay curvatures of jerk, acceleration and velocity. The curvature of the natural decay function of jerk signal propagates to other motion parameters without a significant distortion. This feature greatly simplifies the motion prediction algorithms of AMPP for short-term real-time simulations. For a full scenario of UGV driving from one point to another, only four major acceleration target changes are needed. Momentary acceleration target changes occur also at the correction peaks of a jerk signal. Effects of minor acceleration target changes on acceleration, velocity and distance plots are insignificant.

As seen in Figure 15, AMPP functionality is implemented as Level-2 M-file S-Function. Velocity command is named "In1". Other limits of motion parameters (acceleration limit, jerk limit and distance limit) are named "In2", "In3" and "In4" accordingly. The encoder input simulates data latency but does not simulate quantization noise of a particular encoder.
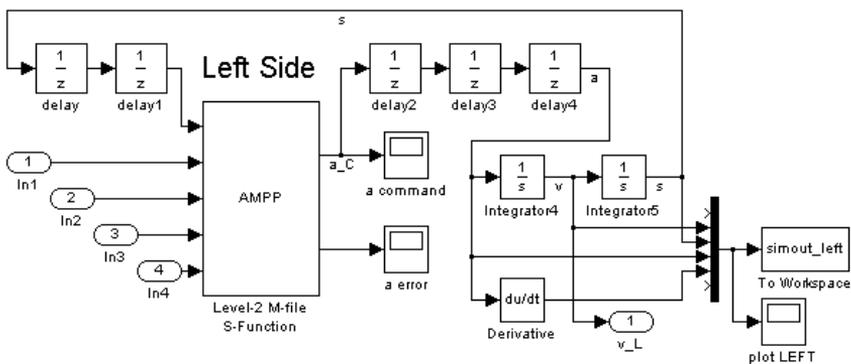
Figure 15. AMPP Simulink block diagram (later used only for the left side)

Velocity, acceleration and jerk in the demonstration software are calculated by the (discrete time) encoder input values. AMPP outputs acceleration command has also added delay.

Start

$i := 1000$

$v < 0$? → yes / no

yes → $v + v_{dec} < 0$? → no

no → $v + v_{dec} > 0$? → yes

$a_{tar} := a_{lim}$

$a_{tar} := 0$

$a_{tar} := -a_{lim}$

$j_n := (a_{tar} - a)/100t_{mc}$

$a_n := a + j_n t_{mc}$

Update other motion parameters

$i <= 0$? → yes / no

End
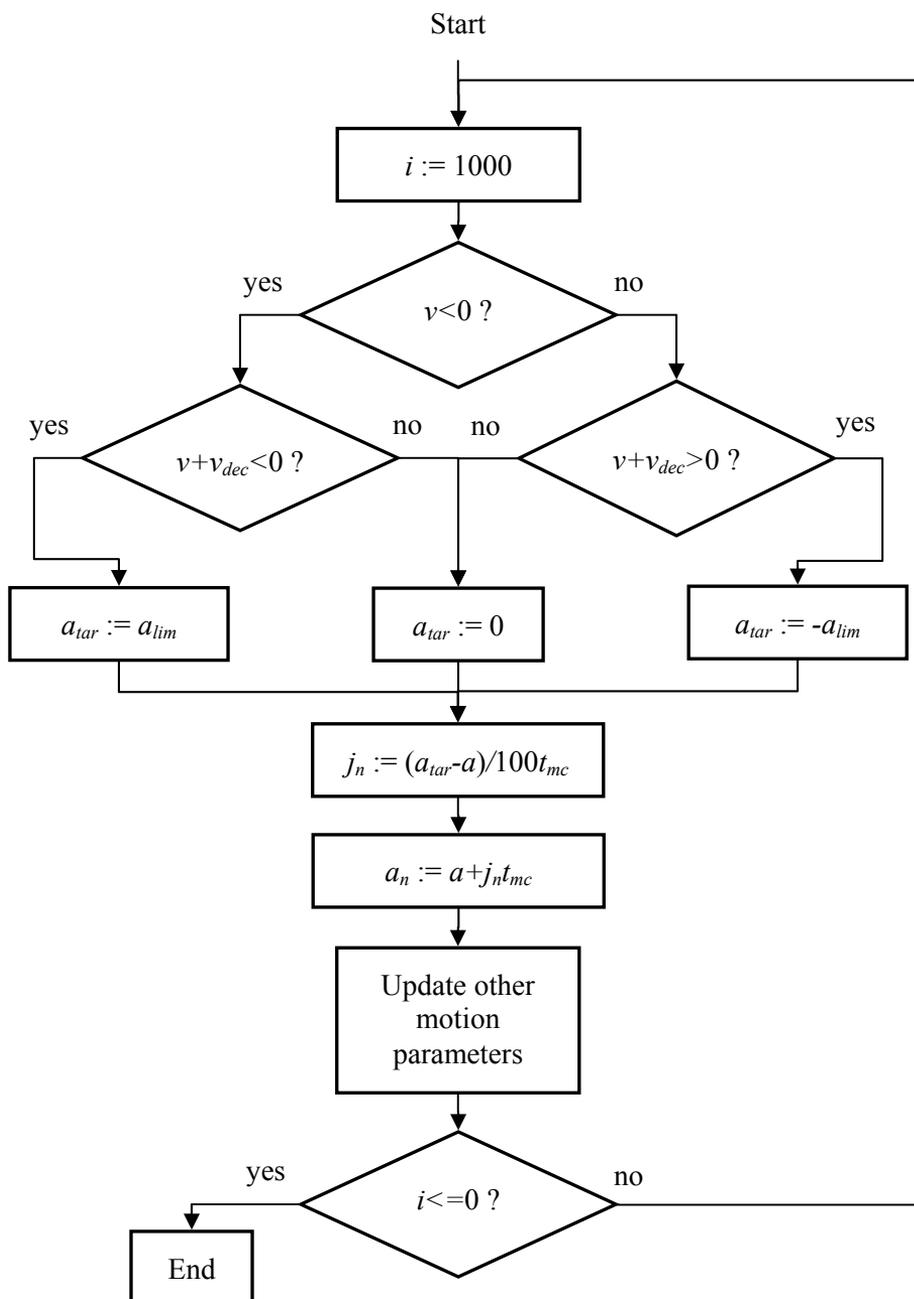
Figure 16. Algorithm for simulating 10 *seconds of velocity magnitude decay*

AMPP uses a motion simulation algorithm (Figure 16) for predicting the stopping point of the nominal REED mode. This algorithm is a simplification and does not consider the velocity tolerance parameter described in later chapters.

Velocity change during the acceleration magnitude decay can be found approximately with the formula:

$$v_{dec} = 100at_{mc}.$$ (3)

Figure 17 shows the simplified algorithm for finding an acceleration output command for the next time-step. Target velocity override and automatic stopping functionality are not shown. Velocity command input is held in the variable v_{tar}. Automatic stopping would override the velocity command input by setting its value to zero.
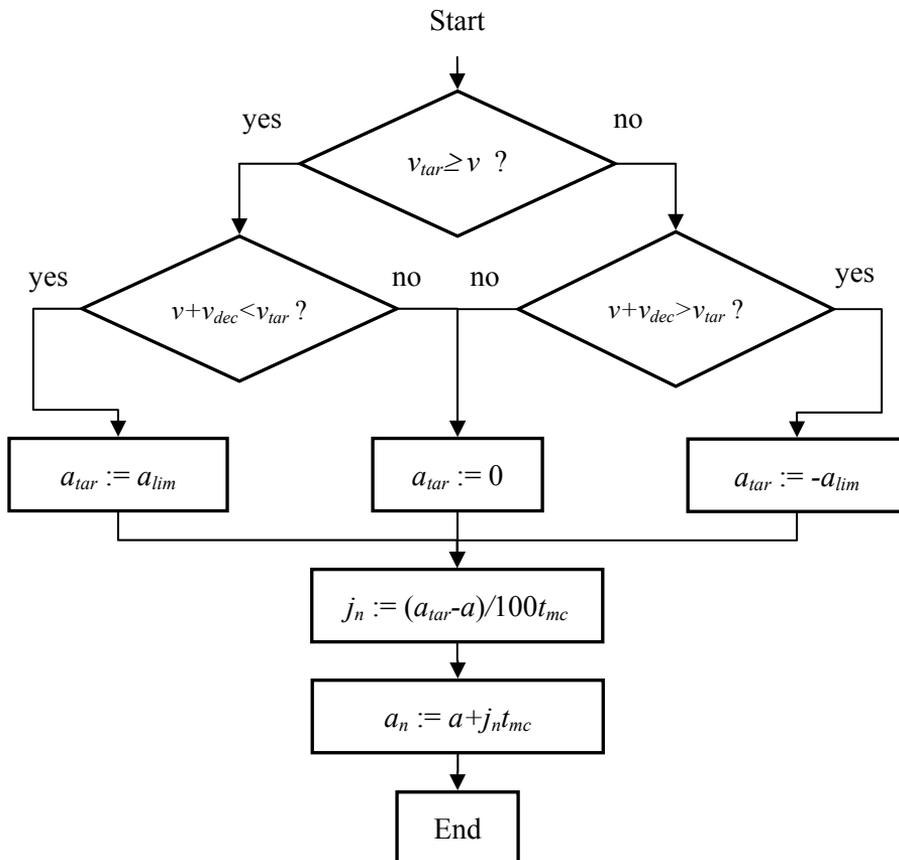
Figure 17. Finding the next acceleration output command

Input data delay and output data delay were introduced into Simulink models to simulate UGV hardware latencies. AMPP modules use command history, detected disturbance and several time-steps of motion simulation, starting from the most recent input data to virtually eliminate such delays. The command sent out by AMPP is always calculated for the future motion according to the number of time-steps the output command propagates to the UGV motion. All output commands are written to first in, first out shifting register ("Command History") and used as soon as relative data is (acquired by the encoder, local positioning system or IMU).
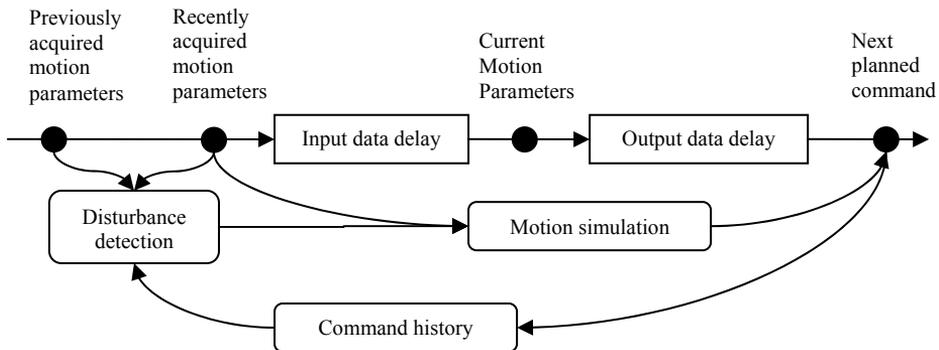
Figure 18. Using command history and disturbance detection for short motion simulation

2.4 Automatic stopping

Because AMPP simulates a normal stopping scenario at every time-step, the stopping distance is known to the UGV on-board software. Depending on the type of Control Station, it may visualize the closest normal stopping point with a marker added to the on-board camera image as an augmented reality effect or just to show the stopping distance in meters as a numeric value.

If the automatic stopping point is set manually, it must be set before the marker covers it. After setting the automatic stopping point, the UGV operator must leave the velocity command constant. AMPP gradually suppresses the velocity command until the vehicle comes to a full stop, as seen in Figure 19.

Simple collision avoidance can use its distance from the obstacle on the path of UGV to automatically adjust the placement of the stopping point. As soon as the distance to an obstacle matches the nominal stopping distance (with a certain tolerance), the target velocity is set to zero and the UGV enters an automatic stopping mode.

In case an obstacle was detected much closer than the predicted stopping point of the REED mode, a normal stopping scenario cannot satisfy the distance limit and the motion planner must switch to an ideal mode.
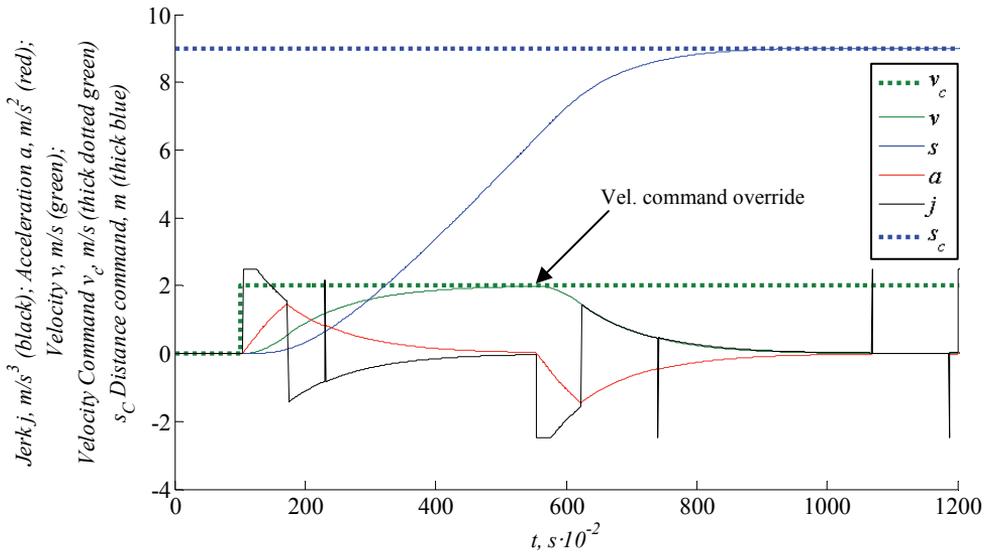
Figure 19. Automatic stopping point and velocity command override

Switching to an ideal mode (Figure 20) uses **default** limits of motion parameters exhaustively for intensified stopping. Intensification of deceleration (by switching to ideal motion planning mode) may be sometimes required only at the first stages of the stopping scenario. As soon as REED simulation satisfies the distance limit, MAPP can switch back to the REED motion planning and make slow and safe arrival to the stopping point.

Emergency stopping mode requires another set of limits. On-board short-term simulation should automatically introduce those, as soon as switching to an ideal mode is not found sufficient. Too intense deceleration may damage the delicate instrumentation and even flip-over the vehicle if it does not consider the motion parameter limits. Emergency stopping set of limits depends mostly on the weight distribution of the UGV on wheel contact surfaces, terrain inclination and absolute maximum ratings (durability) of on-board equipment.

Stopping algorithm is executed every time-step and may switch between motion profile planning modes and motion parameter limits.
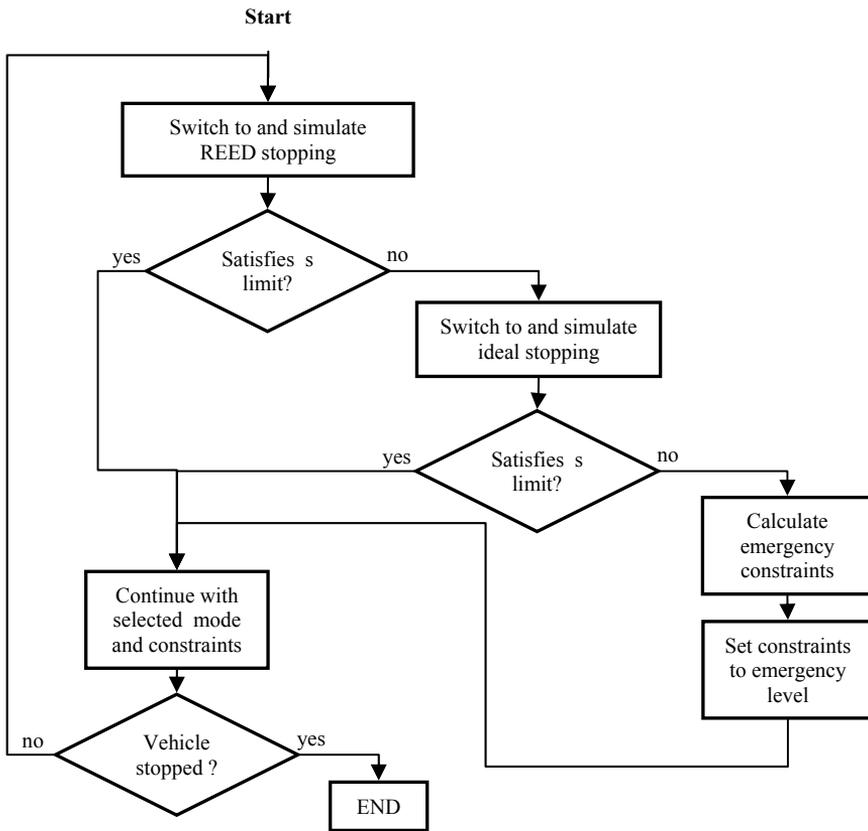
Figure 20. Automatic stopping algorithm

2.5 Gradual change of input velocity commands

In Figure 21 the velocity tolerance is inappropriately low and after velocity has stabilized, noticeable repetitive jerk peaks are present in the jerk command.
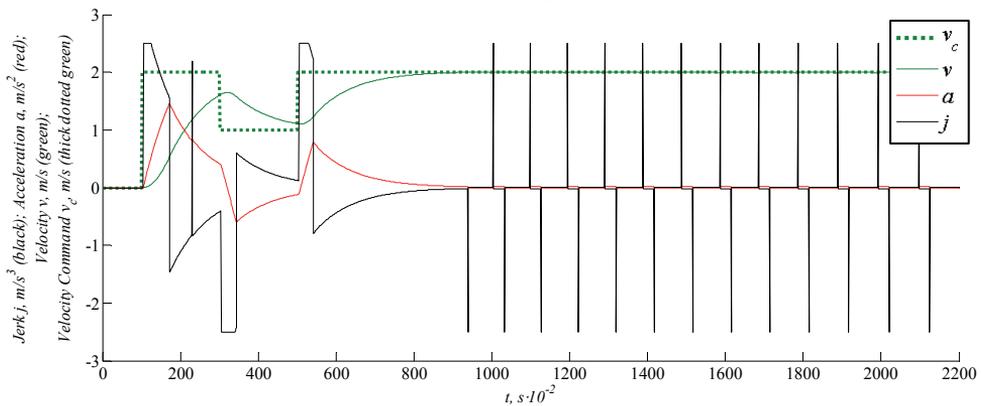
Figure 21. Motion profile with velocity tolerance (±0.001 m/s)

Jerk oscillations occur because AMPP algorithms operate in discrete time and use some model simplifications to reduce the load of CPU (Central Processing Unit). By increasing velocity tolerance to ±0.02 m/s it is sufficient to effectively eliminate jerk oscillations, as shown in Figure 22.
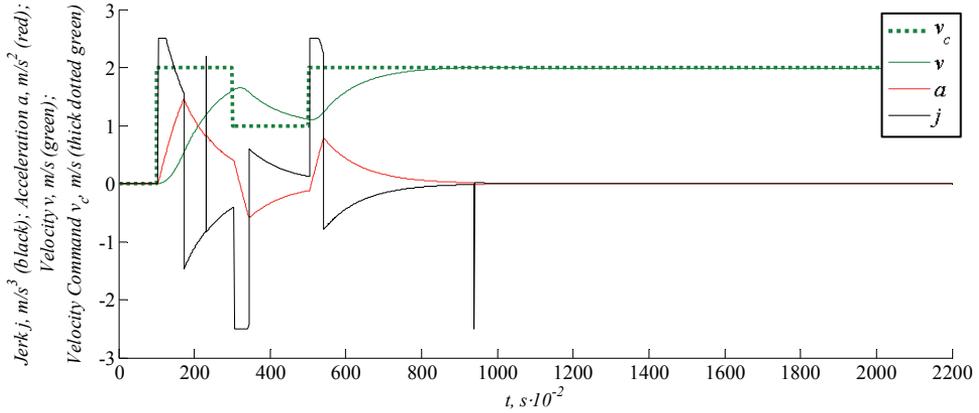
Figure 22. Motion profile with velocity tolerance (±0.02 m/s)

Velocity tolerance removes jerk oscillations. AMPP discrete time software is simple enough to simulate several seconds of motion (stopping scenario) 100 times per second. This solution is considered satisfactory, as in actual UGV motion there will most likely be many unpredictable disturbance peaks and deviations from initially planned motion profiles and trajectories. Many jerk peaks, which are within their limits, are necessary for responsive control.

In some cases it would be useful to widen the tolerance range of velocity even more. For example, repetitive uphill and downhill drive could use some of kinetic energy collected at the previous decent to climb up at the following accent. Long smooth descents would suggest using also regenerative braking, which among other benefits gives more control over braking [37], compared to traditional friction based braking.

Gradually changing input velocity command v_C (Figure 23) is not generally preferable as AMPP does not analyze trends of input velocity command change. Instead, AMPP creates the best fitting motion scenario every time AMPP main cycle is executed (100 s^{-1}). At the input velocity command ramps, the jerk is oscillating in a frequency about 1/3 of the AMPP main cycle execution frequency, but its amplitude remains within permitted jerk limits (Figure 24). Radio links due to their limited bandwidth often limit Control Station of sending more than about 10 commands per second, depending on the chosen baud rate, communication protocol and command set. Actual AMPP output, therefore, would have lower frequency jerk oscillations present when changing the input velocity command gradually.
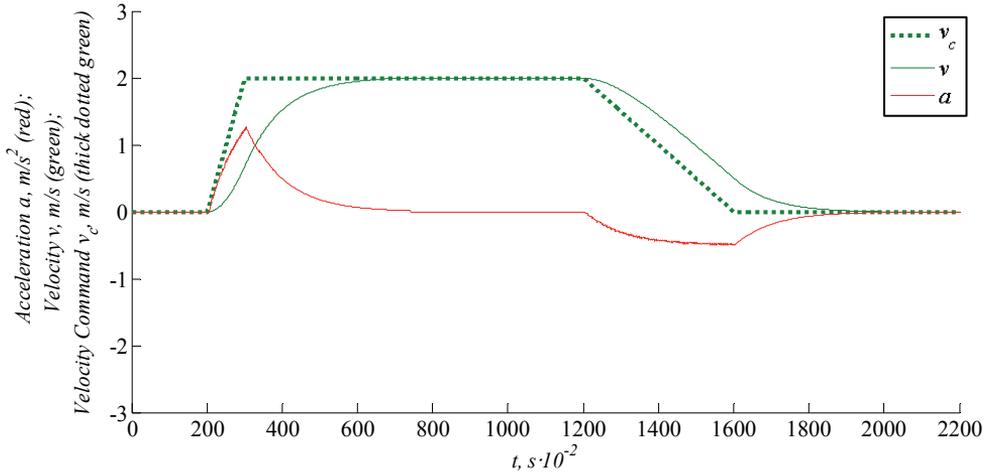
Figure 23. Gradual change of the input velocity command scenario
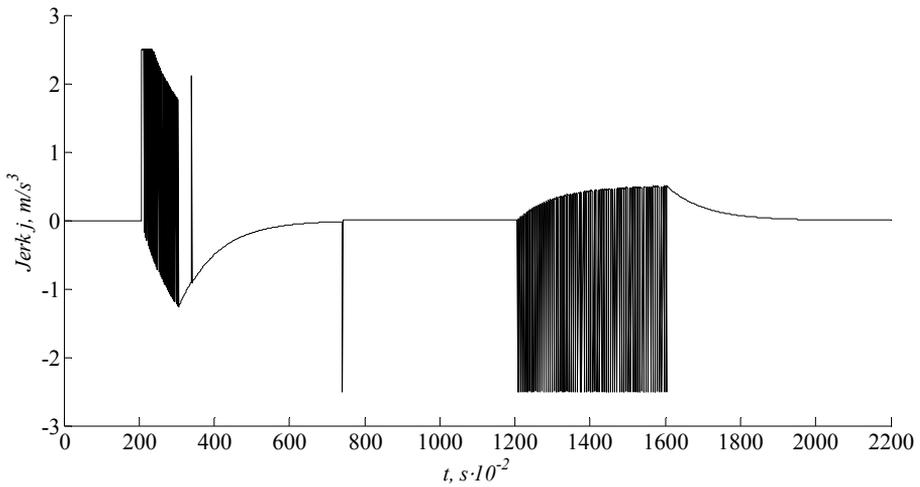
Figure 24. Gradual change of the input velocity command scenario – jerk

Similarly to the dithering effect in image processing, the impact of such oscillations does not cause significant degradation of the acceleration command. It can also be observed that input velocity command ramps stretch out acceleration pulses along the time axis. This stretching effect depends on the slope of the input velocity command ramp.

2.6 Chapter summary

- Methods for straight motion control of the UGV were studied in this section of the thesis.
- REED type of motion profile planning has fast response at the beginning of the motion scenario and extended settling time as motion parameters are nearing the limits of motion parameters.
- Natural decay function of the jerk allows using simplified calculations for short motion simulations, compared to ideal motion planning.
- When the velocity command is changed gradually, instead of rare, large steps, jerk oscillation occurs, which remains in allowed limits and does not deteriorate acceleration (or other type) of output commands notably.
- Ideal motion planning mode uses default limits of motion parameters for intensified stopping.
- Emergency set of limits of motion parameters in an ideal mode may be required to shorten stopping distance.
- More than one AMPP module is necessary for creating motion command sequences for curvilinear motion.

3. MOTION PLANNING FOR CURVILINEAR MOTION

3.1 Turning radius of the skid-steer UGV

Skid-steer type vehicles are well suited for maneuvering in tight spaces. This is where zero-radius turning capability comes handy. In other cases, the space is not of concern and steady pace is preferable to the small turn radiuses. Climbing uphill would suggest using symmetrical drive mode, so skid action does not consume additional energy and the left and right wheels may develop almost equal grip on the uniform terrain. Driving to a docking station should be made by straight motion to have reliable wheel odometry data for smooth and accurate stopping. Driving symmetry helps to distinguish between driving modes, as shown in Table 3.

Table 3. Commonly used drive modes of a skid-steer type UGV

Driving Mode		Skidding	Comment
Symmetric	$v_L = v_R$ $a_L = a_R$ $j_L = j_R$	No	Straight Drive
Non-symmetric	$v_L \neq v_R$ $a_L \neq a_R$ $j_L \neq j_R$	Yes	Varying turn radiuses
Anti-symmetric	$v_L = -v_R$ $a_L = -a_R$ $j_L = -j_R$	Yes	Zero-radius Turn

In this table v_L, v_R – tangential velocity of the left and right side reference points; a_L, a_R – tangential acceleration of the left and right side reference points; j_L, j_R – tangential jerk of the left and right side reference points.

There is a kinematic equivalence between the tread [38] skid-steer vehicle and wheel [5] contact points of an ideal differential drive vehicle. Skid-steer vehicles (either tracked or wheeled) use different velocity ratios for left and right side to cause vehicle to follow arcs with certain radiuses. Instead of describing UGV's curvilinear motion with an array of turning radiuses (which can only be positive), it is more convenient to use r_{COR} to describe the instantaneous displacement of the COR (Center Of Radius) from the center of the UGV to the left. It has the same magnitude as turn radius but it can distinguish left and right turns by its sign. Positive value of r_{COR} denotes turning to the left (positive angular velocity of the UGV frame), negative to the right (negative angular velocity of the UGV frame).

In a virtual model of the UGV, COR can only be on the line [4], which connects the reference points of the left and right side. In case the tangential velocities of reference points are equal, r_{COR} is considered irrelevant and not calculated. In other cases, displacement of COR can be calculated by the formula:

$$r_{COR} = \begin{cases} \pm\infty, & \text{if} \quad v_R = v_L \\ \dfrac{l(v_L + v_R)}{2(v_R - v_L)}, & \text{if} \quad v_R \neq v_L, \end{cases} \tag{4}$$

where r_{COR} − displacement of COR to the left side of the UGV; l − track width (distance between the left and the right reference point).
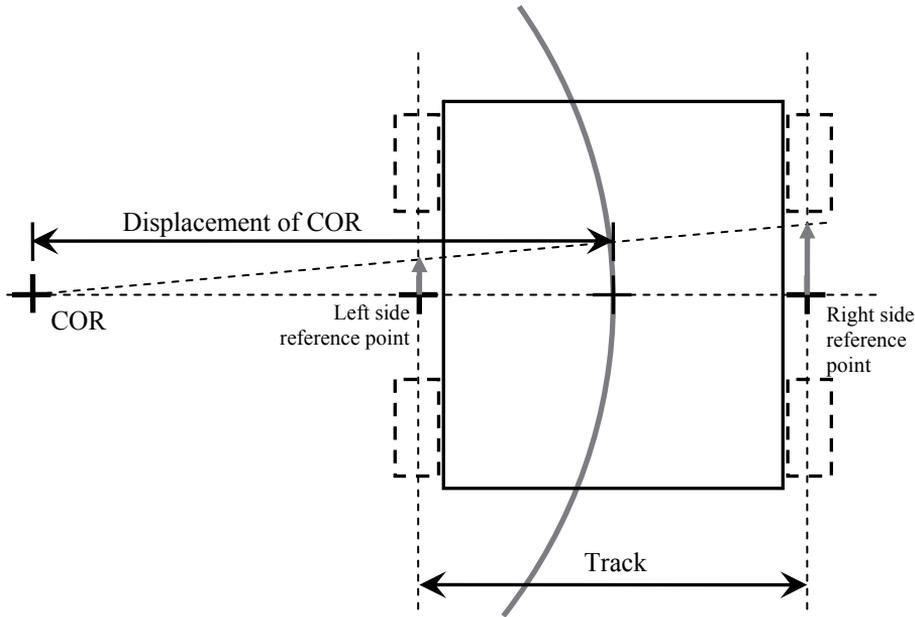
Figure 25. Track, reference points and COR (positive r_{COR} presented)

In actual UGV control, tire physics, uneven weight distribution and possibly uneven terrain properties are involved, which means that making turns with particular radiuses would require LLMCL intervention and AMPP corrections based on the motion feedback data.

3.2 Theoretical trajectory of the UGV according to raw input data

When straight motion of the UGV switches into turning with a fixed radius, there will be sudden centripetal acceleration applied to the CA. Sudden acceleration change occurs also when the UGV exits the same turn. Virtually instantaneous angular velocity change of UGV wheels and UGV chassis would require

unrealistic angular acceleration peaks, not to mention the damage to the wheel gearboxes and instrumentation.

Such trajectory (Figure 26) could be followed by smoothly stopping the UGV before entering and before leaving every turn, but this would unnecessarily extend the time of drive and increase total energy consumption (compared to steady pace alternatives).

Figure 26 also illustrates trajectory and displacement of COR r_{COR} after every 0.3 s, describing curvature properties and velocity of the UGV in one plot. UGV front is initially oriented to the Axis x ($\theta = 0$). The starting point is point zero of both axes.
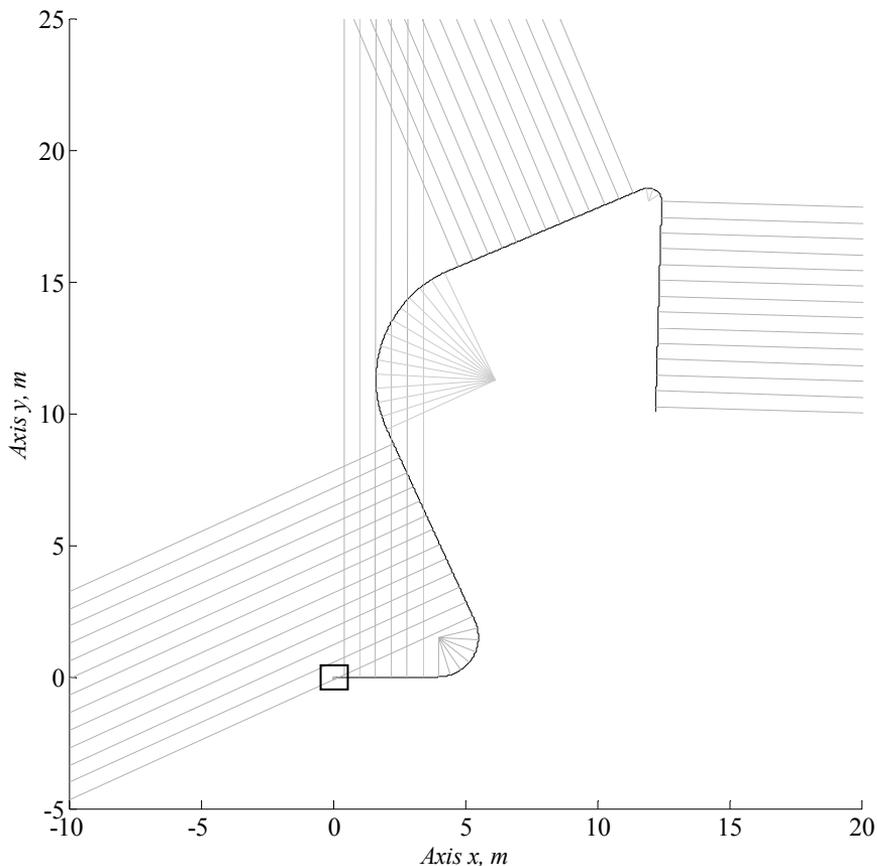
Figure 26. UGV trajectory with turn radius shown every 0.3 s – raw input

Raw input control is not suitable for UGV trajectory generation because following such trajectory at a relatively steady pace would introduce high jerk peaks. The trajectory in Figure 26 was created from raw input velocity commands of Figure 28 and 29.

3.3 Dual-AMPP trajectory

To create a more usable trajectory and motion profiles, two AMPP control blocks (one for each side, as in Figure 27) can be used. Limits of motion parameters are the same as in previous AMPP example scenarios.
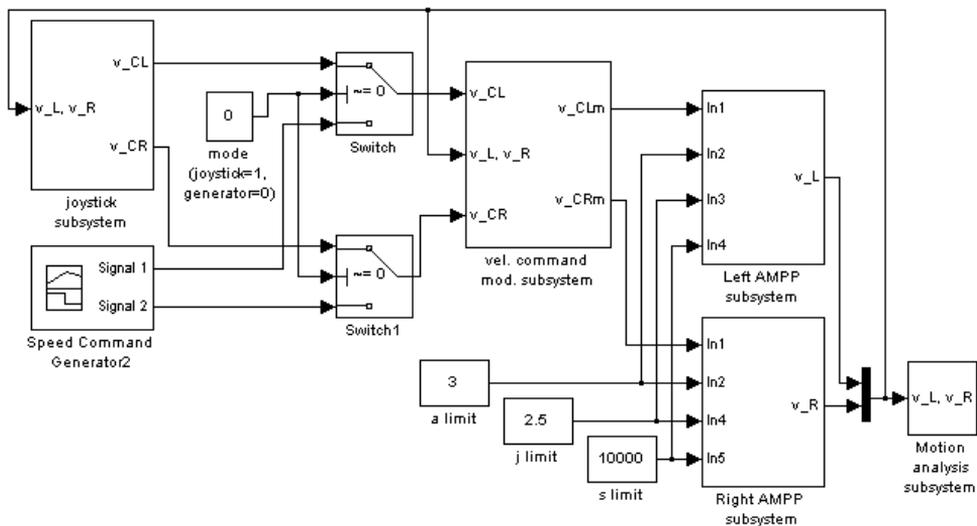
Figure 27. Simulink block diagram of Dual-AMPP control

In the following example (Figure 28 and 29), neither of the input velocity commands v_C nor tangential velocities v of reference points have negative values at any moment of time. This limitation is useful as it reduces angular velocity ω of the UGV frame to half of its normal range.

Subsystems like "joystick subsystem" and "velocity command modification subsystem" are described as block diagrams in the following chapters.
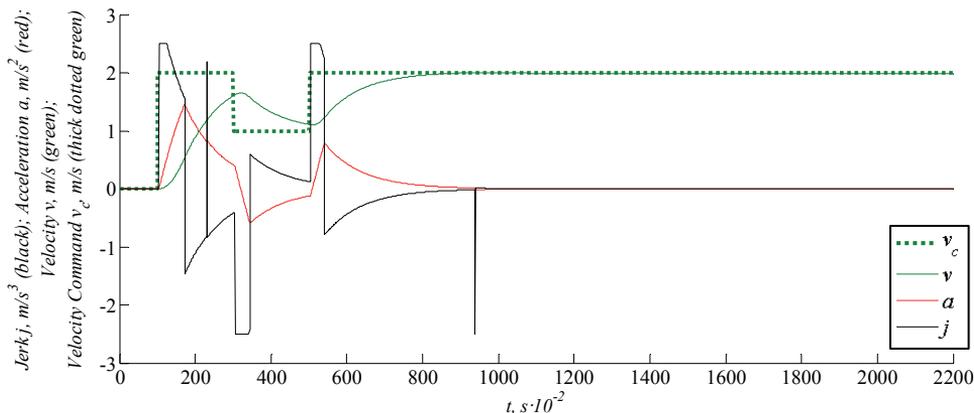
Figure 28. Input velocity command and tangential motion of the left side
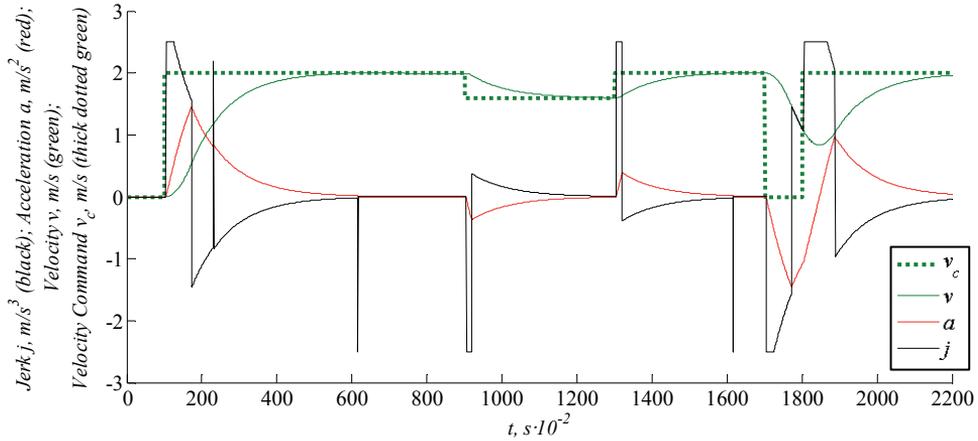
Figure 29. Input velocity command and tangential motion of the right side

Input velocity command (Figure 28 and 29) is changed rarely and with large steps to illustrate the extremities of motion, keeping the default set of motion parameter limits. Because the UGV can be controlled by inputting rarely changing velocity commands, extensions to MP can be made, which finds the best timing and levels for velocity command pulses to make turning semi-autonomous. Such extension to local path planning would combine smooth driving with the capability to automatically drive around obstacles, instead of just stopping before the collision.

Long-range path planning trajectories could be assessed by extended MP simulations, which can estimate the time of drive, which is dependant not only on the length of the path and properties of the terrain but also on the shape (jaggedness) and width of the path. Tangential velocity of both reference points must be reduced to make sharp turns without violating maximum acceleration magnitude limit.

As seen in Figure 30, by following Dual-AMPP motion profiles, the UGV switches smoothly between straight sections and curves, input by two rough input velocity command sequences. Displacement of COR is presented by grey lines after every 0.3 s, which helps to estimate the UGV velocity. Three markers ("I", "II" and "III") help to match local maximums of acceleration components at the center of the UGV. Virtual UGV frame is shown at the starting position.
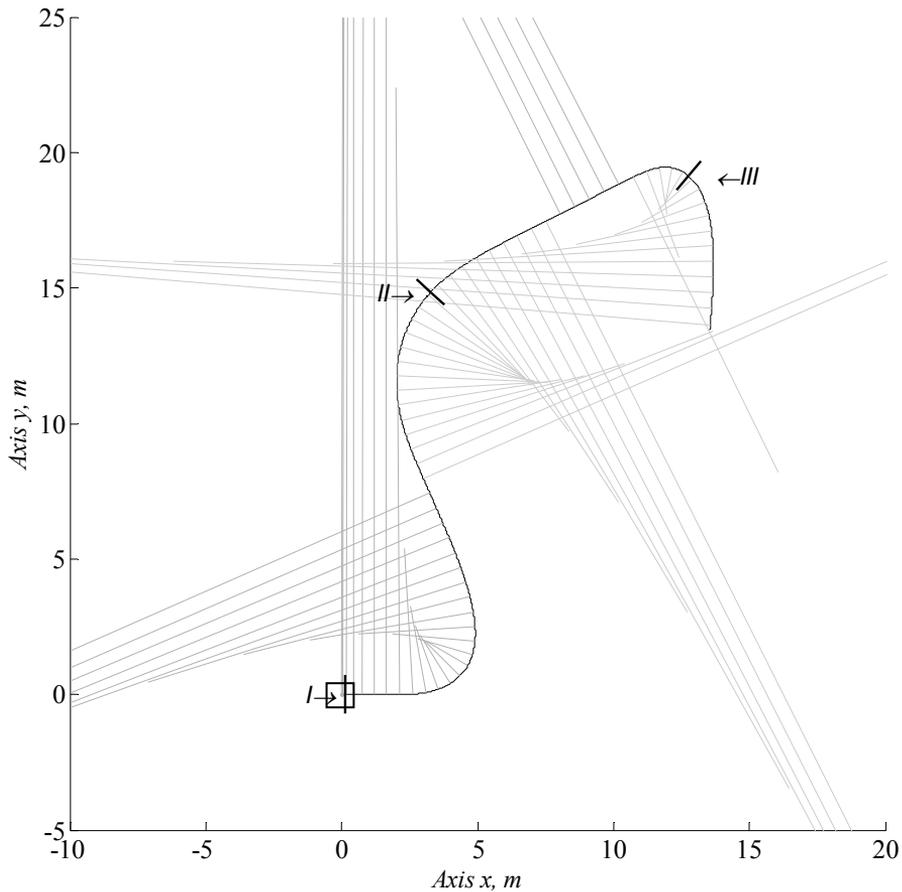
Figure 30. UGV trajectory with turn radius shown every 0.3 s

3.4 Acceleration components at the center of the UGV

It is assumed that the UGV center of weight in a virtual model is concentric with the geometric center of the vehicle. Plot-out of tangential and radial acceleration illustrates how tangential motion of each side propagates to the center of the UGV. Also, some of the unique characteristic curvatures can be identified.

The first marker ("I" in Figure 31) shows a point in time where the UGV accelerates driving straight and thus the radial component of acceleration is zero. The second marker ("II") notes curvilinear motion with stabilized turn radius and, therefore, almost constant radial acceleration component. The third marker ("III") demonstrates how significant tangential and radial acceleration components are both present when slowing down only one side of a vehicle and considering only the center of the UGV.
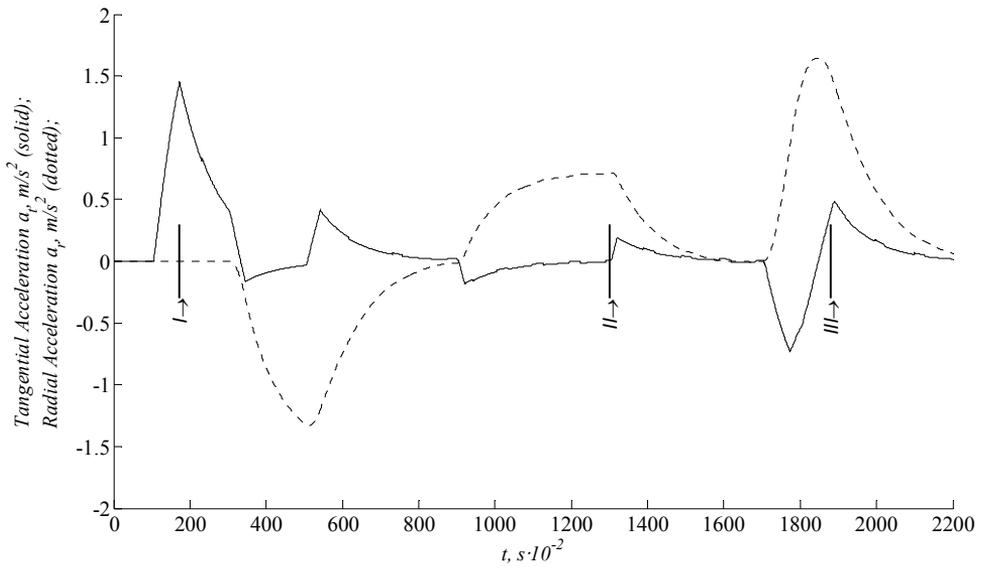
Figure 31. Acceleration components at the center of the UGV

The same three markers on the COR displacement plot (Figure 32) illustrate the effect of smaller radius turns (markers II and III) at virtually constant velocity. Entering curves is faster than exiting them, so it is possible to make fast turns to dodge some obstacles. Slow exiting from turns may have a damping effect for some specific low frequency oscillating equipment (like possibly some antenna systems).
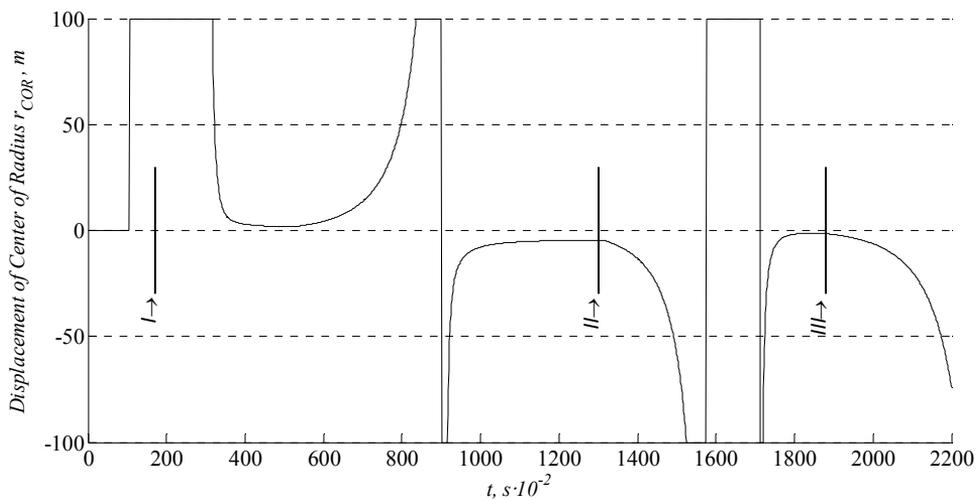
Figure 32. Displacement of COR (cropped to $\pm$ 100 m)

Lateral acceleration measurement at the center of the weight of the UGV provides useful information about possible tire/terrain grip loss at certain levels. It is, however, inadequate for estimating the motion of all CA points. For example, zero radius centripetal acceleration is not present at the CA center. The formation of the highest magnitude acceleration vector within CA is studied in the next chapters along with the UGV control algorithms to keep it within prescribed limits.

3.5 Anti-symmetric and non-symmetric motion

At the beginning of this scenario (Figure 33 and 34), the UGV makes some anti-symmetric zero-radius turns and proceeds at the 7th second with small radius drive sections, intentionally contributing to the most critical motion of CA.
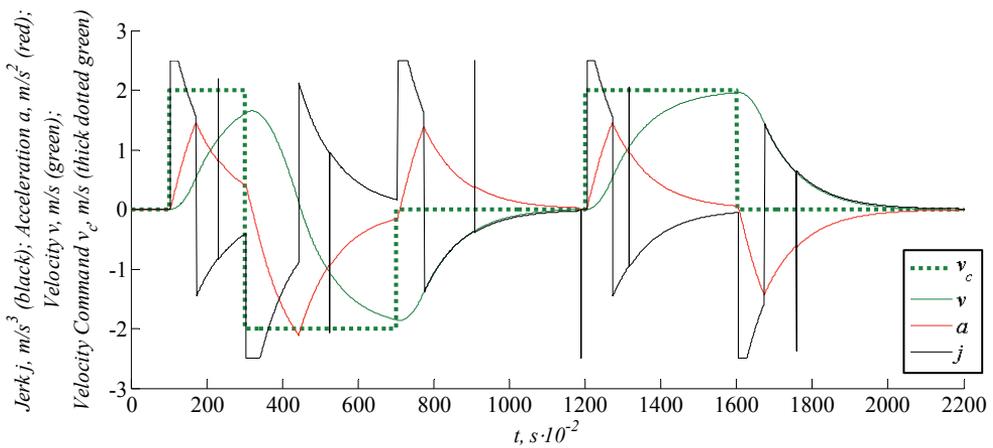
Figure 33. Anti- and non-symmetric motion – left side
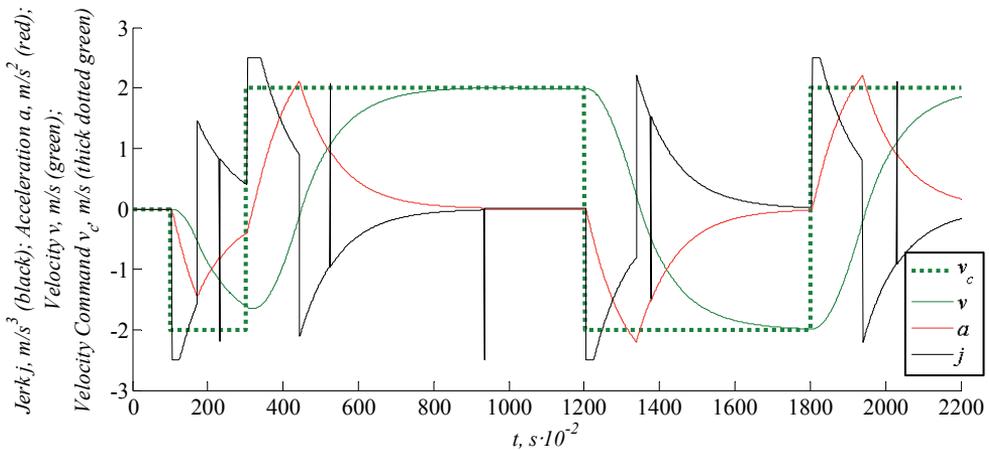
Figure 34. Anti- and non-symmetric motion – right side

Figure 35 demonstrates the displacement of solenoidal vector field circulation points from the center of the UGV to the left, which are r_{COR}, r_{CORa} and r_{CORj} accordingly. In anti-symmetric motion, all circulation points coincide with the center of the UGV.
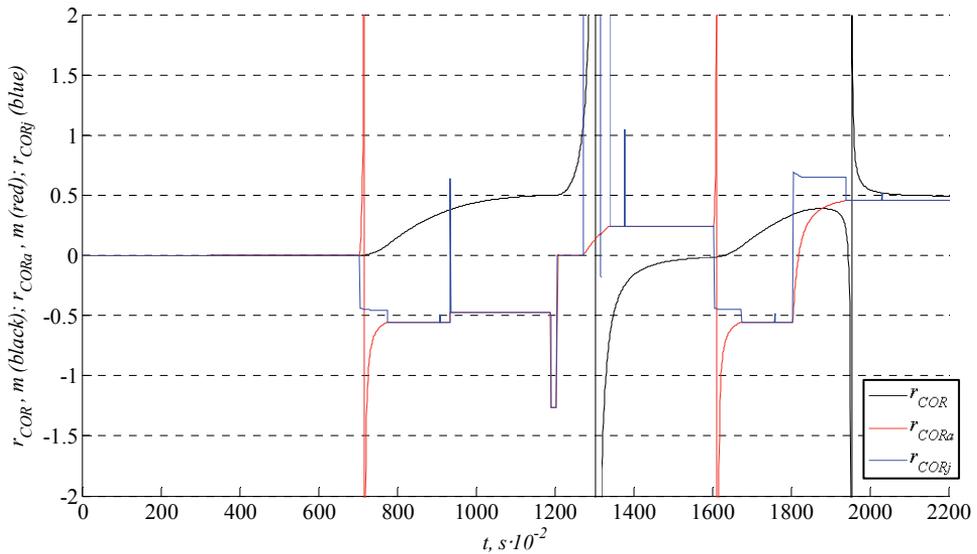
Figure 35. Plot of circulation point displacements r_{COR}, r_{CORa} and r_{CORj}
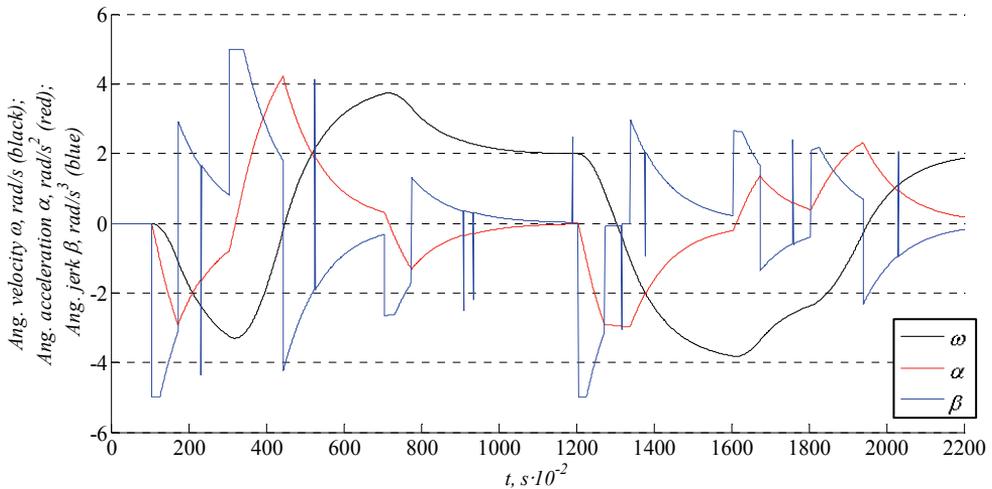
Figure 36. Plot of angular velocity, angular acceleration and angular jerk

As seen in Figure 36, angular jerk, angular acceleration and angular velocity share some similarities with either side of tangential jerk, tangential acceleration and tangential velocity, accordingly.

As Figure 37 is a motion analysis trajectory plot, it does not visualize zero-radius turning at the beginning of this driving scenario. Spiraling trajectory line starts at the point zero of both axes when anti-symmetric motion evolves to non-symmetric motion by slowing down the velocity of the UGV left side reference point. The UGV frame is shown at the starting position.
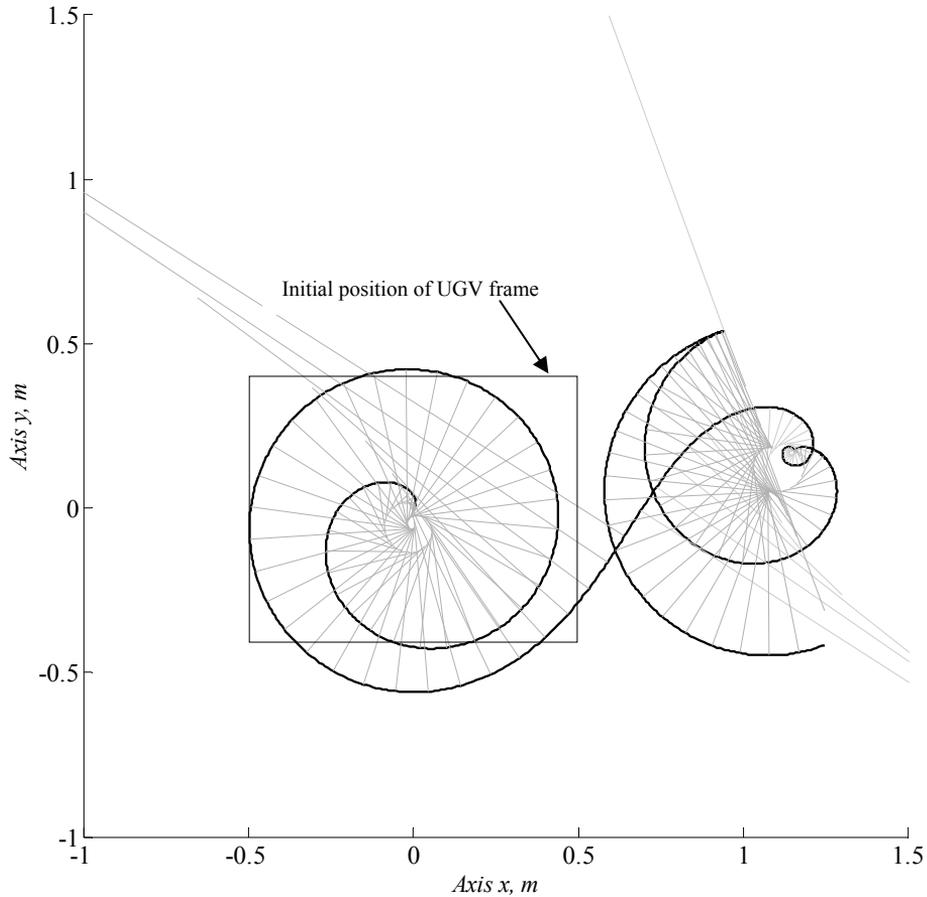
Figure 37. UGV Trajectory with turn radius shown every 0.1 s – critical motion

3.6 Chapter summary

- Dual-AMPP control method was proposed in this section of the thesis.
- Raw user input trajectories are unsuitable for low impact safe UGV control.
- Dual-AMPP control method without further development fails to keep maximum acceleration magnitude within prescribed limits.

4. REDUCTION OF MAXIMUM ACCELERATION

4.1 Motion of the UGV frame

Similarly to tangential velocity components of the reference points defining the displacement of COR (r_{COR}), tangential acceleration components of the same points define the displacement of the center of the circulation point of solenoidal vector field. Displacement of the minimum magnitude point (circulation point) of this vector field, which is caused by tangential acceleration of the left and right side reference points, can be calculated by:

$$r_{CORa} = \begin{cases} \text{undefined}, & \text{if} \quad a_R = a_L \\ \dfrac{l\left(a_L + a_R\right)}{2a_R - 2a_L}, & \text{if} \quad a_R \neq a_L, \end{cases} \tag{5}$$

where r_{CORa} – displacement of the minimum magnitude point of the tangential acceleration vector field.

Displacement of the minimum magnitude point (circulation point) of the jerk vector field (caused by tangential jerk of the left and right side) can be calculated by:

$$r_{CORj} = \begin{cases} \text{undefined}, & \text{if} \quad j_R = j_L \\ \dfrac{l\left(j_L + j_R\right)}{2j_R - 2j_L}, & \text{if} \quad j_R \neq j_L, \end{cases} \tag{6}$$

r_{CORj} – displacement of the minimum magnitude point of the tangential jerk vector field.

Because tangential components of velocity, acceleration and jerk of each side can be controlled independently, those centers (r_{COR}, r_{CORa}, r_{CORj}) rarely coincide.

Angular motion of the UGV frame is calculated by:

$$\omega = \frac{v_R - v_L}{l}, \quad \alpha = \frac{a_R - a_L}{l}, \quad \beta = \frac{j_R - j_L}{l}, \tag{7}$$

where ω – angular velocity; α – angular acceleration; β – angular jerk of the UGV frame.

4.2 Formation of vector fields

In the analysis of the vector fields created by the tangential motion of the left and right reference points, the highest magnitude vectors are farthest from the center of the UGV in anti-symmetric motion. The circulation points of all such vector fields coincide with the center of the UGV. The magnitude of any vector within the CA, which is marked with red solid line in Figure 38a, can be equal or less than the magnitude of the tangential motion parameter of either side reference point. The center of the CA, in this case (disregarding other possible factors) is clearly safest for critical loading.

(a)   *(b)*

(c)
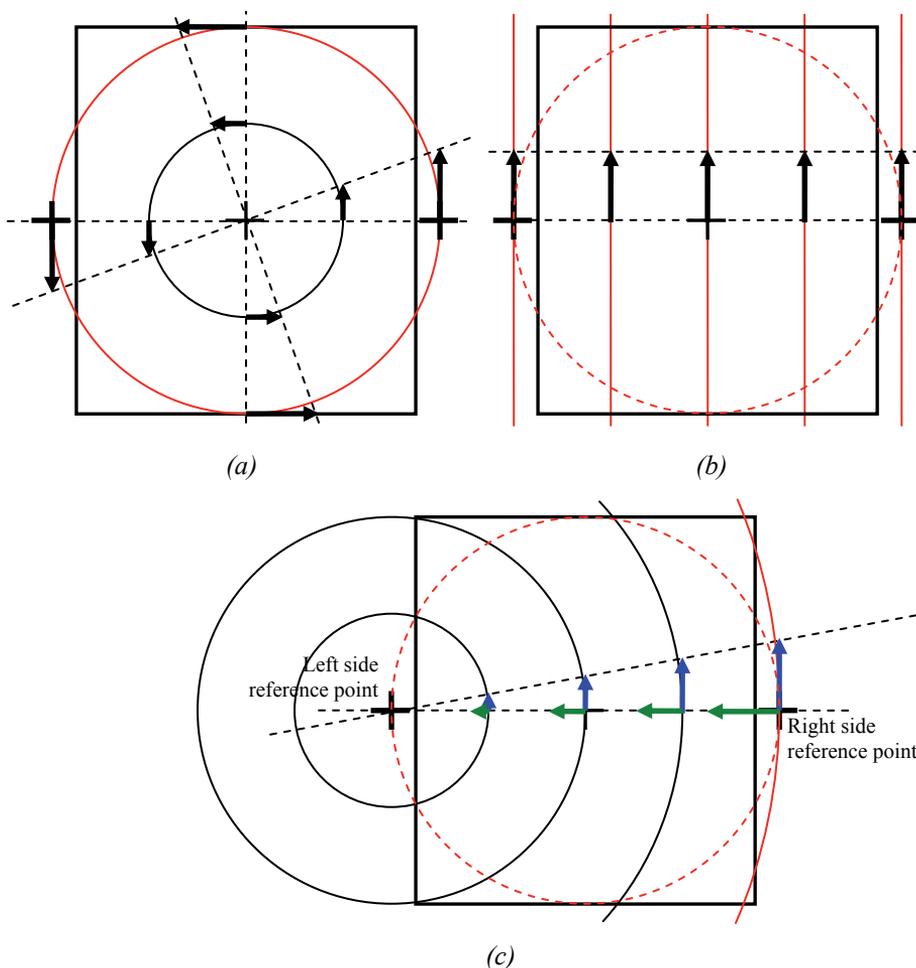
Figure 38. Formation of vector fields: (a) solenoidal vector field of the CA at zero-radius turning; (b) homogeneous vector field at straight drive; (c) solenoidal vector field of velocity and converging vector field of centripetal acceleration

If motion parameters (tangential velocity, tangential acceleration or tangential jerk) of the left and right reference points are equal, the CA is coherent and angular motion parameters are not present, as shown in Figure 38b. In this mode, all points of the CA are equally unfavorable but within safe AMPP limits (disregarding other possible factors). Straight motion represents an exception, where modules, which extend over the CA, do not suffer from worse motion parameters than instruments within the CA.

Figure 38c demonstrates one possible combination of the velocity vector field (with blue vectors) and the centripetal acceleration vector field (with green vectors).

At reference points of the left and right side, radial (centripetal acceleration) and tangential acceleration vectors are perpendicular. From radial acceleration components it is possible to calculate converging acceleration vector field at every point that moves along with the UGV frame. From tangential acceleration components, measured by IMUs, it is effortless to calculate the solenoidal acceleration vector field. Total acceleration field formation, minimum magnitude point disposition and maximum acceleration of CA is addressed in further chapters.

Straight motion can be viewed as a solenoidal field with the center at infinity. However, as motion becomes symmetric, it is easier for UGV algorithms to switch to another set of much simpler formulas for vector field analysis.

4.3 Acceleration vector fields at anti-symmetric motion

Zero-radius turns are almost unavoidable when operating in tight spaces. The following analysis uses Dual-AMPP drive with default limits (v_{max} = 2 m/s, a_{lim} = 3 m/s^2 and j_{lim} = 2.5 m/s^3) to the left and right side tangential motion parameters.

Applying maximum velocities (v_L = 2 m/s, v_R = −2 m/s) to the reference points of the UGV frame, the angular velocity (ω = −4 rad/s) creates an irrotational vector field of centripetal acceleration around the center of the UGV, as shown in Figure 39a.

(a)   *(b)*

(c)
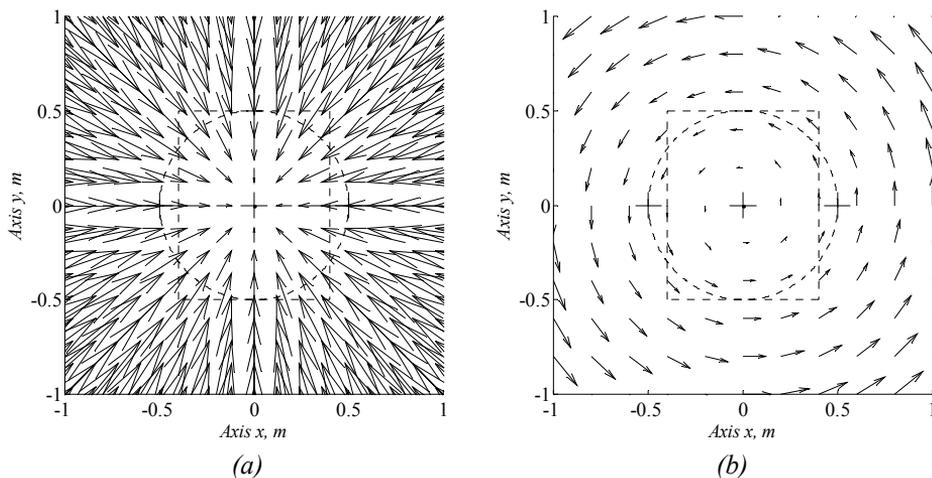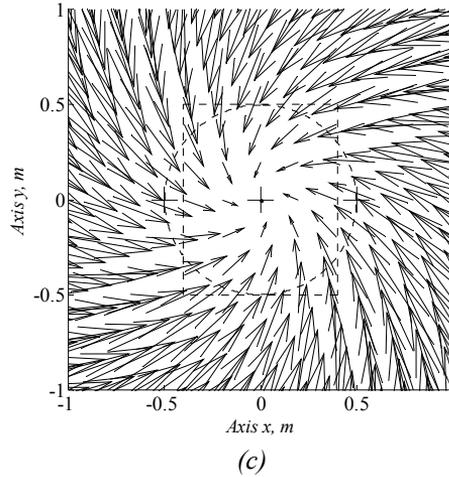
Figure 39. Analysis of anti-symmetric motion: (a) converging vector field of centripetal acceleration ($\omega = -4$ rad/s, $r_{COR} = 0$ m); (b) solenoidal vector field of angular acceleration ($\alpha = 6$ rad/s^2, $r_{CORa} = 0$ m); (c) vector field ($\omega = -4$ rad/s, $\alpha = 6$ rad/s^2, $r_{COR} = 0$, $r_{CORa} = 0$ m)

Angular velocity ω of the UGV frame introduces the radial acceleration ($a_r = \omega^2 r_\omega$) vector field. Radius r_ω is a distance from the point of interest to the center of the convergence point.

Tangential acceleration components ($a_t = \alpha r_\alpha$) rely on the distance to the angular acceleration axis r_α. In anti-symmetric motion (perfect zero-radius turning) the axis of angular velocity and the axis of angular acceleration coincide with the center of the UGV ($r_{COR} = 0$ m, $r_{CORa} = 0$ m).

When instantaneously applying tangential acceleration $a_L = -3$ m/s^2, $a_R = 3$ m/s^2 to the reference points, the plot looks like in Figure 39b ($\alpha = 6$ rad/s^2). This creates a solenoidal vector field with the circulation point coinciding with the center of the UGV.

Due to the jerk limit, AMPP with default limits does not allow acceleration to be increased to its maximum level instantaneously and such clean solenoidal vector field is not attainable.

When angular acceleration and angular velocity are both at their maximum, the vector field plot presented in Figure 39c shows the acceleration vectors considering both factors (maximum ω and α). A similar situation may occur when the UGV is rotating clockwise with full angular velocity (–4 rad/s) and suddenly (disregarding jerk limits) applies maximum angular acceleration (6 rad/s^2) counteracting the angular velocity.

As seen in Figure 39c, the complementary effects of angular acceleration on the angular velocity are minor. All edges of the Critical Area suffer total acceleration of equal magnitude, mostly defined (using default motion parameter limits) by

angular velocity. Tangential and radial components of acceleration in this case are perpendicular.

4.4 Acceleration vector fields at non-symmetric motion

As the circulation point of the tangential acceleration vector field and the convergence point of the radial (centripetal) acceleration vector field are separated, angles between radial and tangential components vary along the CA. Scenarios where those two points coincide with the left and right reference points are common practice when maneuvering the vehicle in tight spaces.
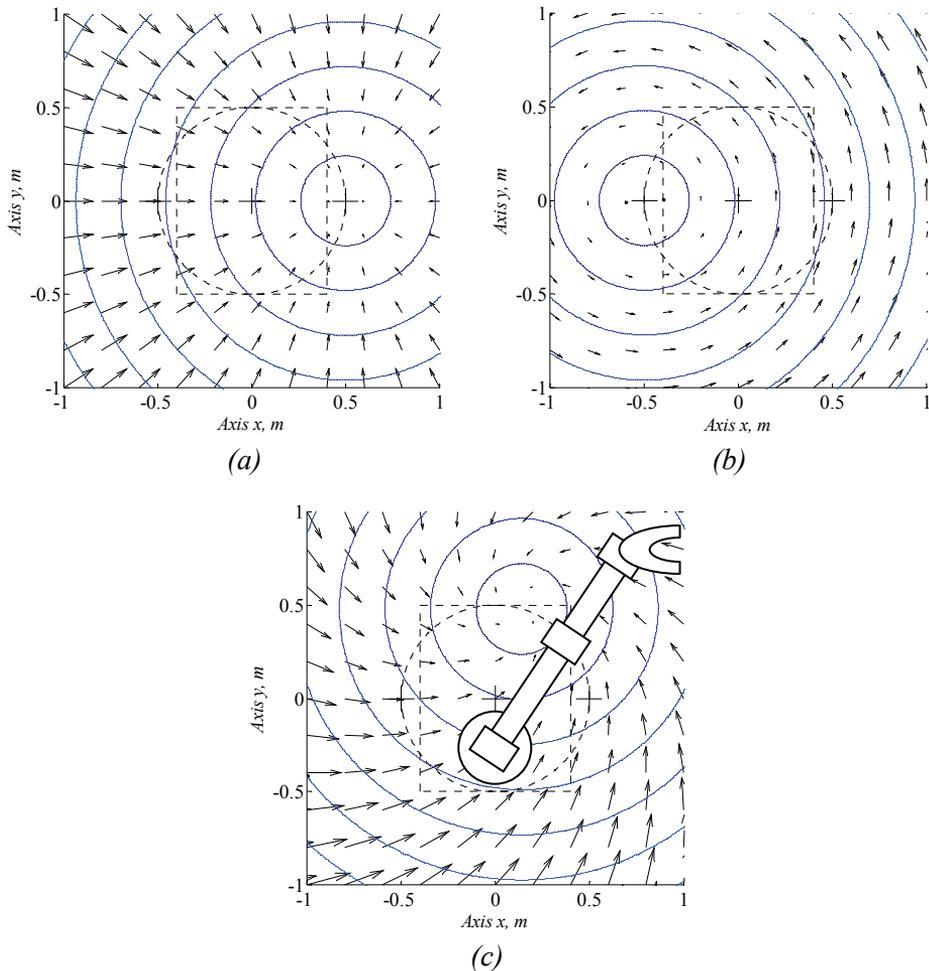
Figure 40. Analysis of non-symmetric motion: (a) converging vector field of centripetal acceleration ($\omega = -2$ rad/s, $r_{COR} = -0.5$ m); (b) solenoidal vector field of angular acceleration ($\alpha = 3$ rad/s^2, $r_{CORa} = 0.5$ m); (c) vector field ($\alpha = 3$ rad/s^2, $r_{CORa} = 0.5$ m, $\omega = -2$ rad/s, $r_{COR} = -0.5$ m)

Figure 40a shows the centripetal acceleration vector field when the left side has maximum velocity (v_L = 2 m/s) and the right side has tangential velocity (v_R = 0 m/s). That situation represents a displacement of COR r_{COR} = 0.5 m. Because angular velocity was halved (compared to the previous example) by changing the right side velocity to zero, the magnitude of the centripetal acceleration (assuming the same distance from the convergence point) dropped 4 times compared to the anti-symmetric motion. As the maximum distance from the convergence point in the CA was increased only 2 times, the maximum acceleration magnitude in its highest point is 2 times lower than in the previous example of the centripetal acceleration vector field.

Tangential accelerations of the left side reference point a_L = 0 m/s^2 and the right side a_R = 3 rad/s^2 would represent the displacement of the acceleration center r_{CORa} = 0.5 m.

Adding tangential and radial vector fields shown in Figure 40b demonstrates how the safest point of the Critical Area develops almost at the front of the UGV. Changing α or ω^2 or both (provided the circulation point and convergence point do not move) changes the placement of the safe but it always stays at the perimeter of the CA. The most critical point of the CA is always the farthest from the minimum magnitude point. In this case (r_{COR} = −0.5 m and r_{CORa} = 0.5 m) the distance from the safest point to the farthest edge of the CA is equal to the CA diameter (1 m).

As seen in Figure 40c, the minimum magnitude point of the total acceleration field is shifted along the x and y-axis of the UGV coordinate system. Solenoidal and converging components are both noticeable. Some specific devices may reach outside the CA. Figure 40c also illustrates a robot manipulator which happens to be close to the minimum magnitude point. However, the analysis of the acceleration vector field can be easily extended to a larger circle, as seen by the formulas in the following chapters.

Because the formation of acceleration vector fields is sometimes counter-intuitive, it would be useful to visualize the vector field of the CA on the screen of the UGV Control Station at UGV control training.

4.5 Acceleration caused by the tangential motion of reference points

If the maximum magnitude of acceleration within the CA is caused only by centripetal acceleration, it can be calculated by the formula:

$$a_{max} = \frac{1}{2l}\left[\left|v_R{}^2 - v_L{}^2\right| + \left(v_R - v_L\right)^2\right],\tag{8}$$

where a_{max} – maximum acceleration magnitude within the CA.

If the tangential acceleration of the left and right reference points and the resulting circular acceleration vector field is disregarded, UGV control algorithms could use this formula for keeping maximum acceleration magnitude within limits by

excluding certain parts of the input velocity command space from usage. Isolines of Figure 41 describe the possible thresholds for excluded sets at different maximum acceleration magnitude limits.
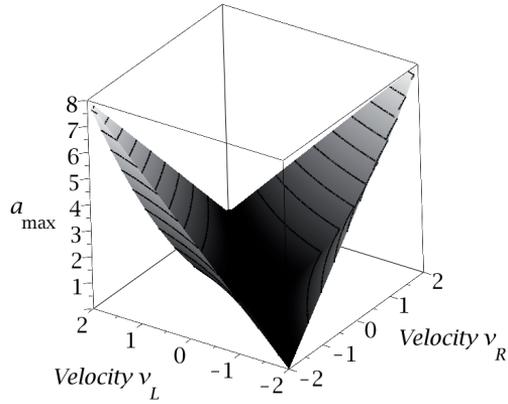
Figure 41. Maximum centripetal acceleration caused by tangential velocities (l = 1 m)

As seen in Figure 41, particular velocity combinations cause high maximum acceleration within the CA, while others do not.

Tangential acceleration of the left and the right side create the highest magnitude acceleration in the most critical point of the CA by the following formula:

$$a_{max} = \frac{1}{2}\left(\left|a_L - a_R\right| + \left|a_L + a_R\right|\right) = \max\left(\left|a_L\right|, \left|a_R\right|\right). \tag{9}$$
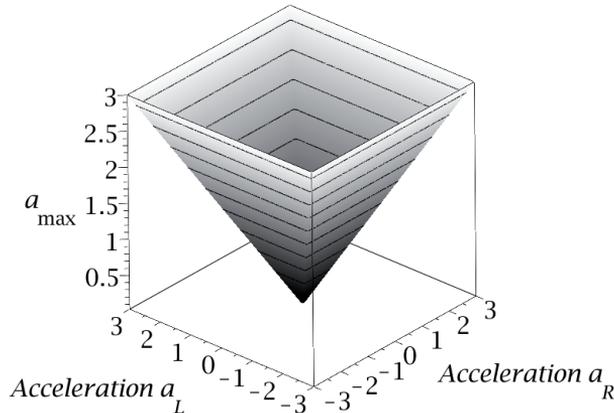
Figure 42. Maximum acceleration caused by tangential accelerations (l = 1 m)

Figure 42 demonstrates the most critical combinations of tangential accelerations. The highest magnitude of total acceleration within the CA is defined by the left or right tangential acceleration, whichever has a higher magnitude.

4.6 Highest magnitude acceleration within the Critical Area

The following schematic (Figure 43) illustrates many relationships between the symbols needed to find the offset of the minimum magnitude point of the total acceleration vector field and its distance to the farthest point within the CA.
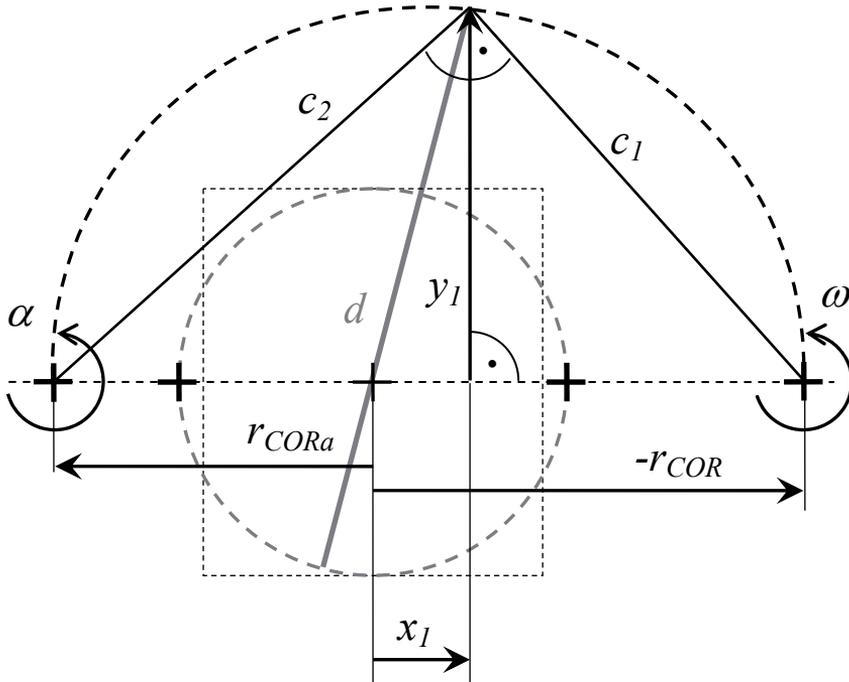
Figure 43. Minimum magnitude point offset (negative r_{COR} has been presented for a better overview)

A set of formulas were used in "Motion analysis subsystem" to create plots of the magnitude of maximum acceleration at the most critical point of the CA and to find a method of keeping it within prescribed limits:

$$c_2 = \frac{\left| r_{COR} - r_{CORa} \right|}{\sqrt{1 + \dfrac{\alpha^2}{\omega^4}}}, \tag{10}$$

$$c_1 = \frac{|\alpha| c_2}{\omega^2}, \tag{11}$$

$$y_1 = \frac{c_1 c_2 \alpha}{(r_{CORa} - r_{COR})|\alpha|}, \tag{12}$$

$$x_1 = -r_{COR} + \frac{\sqrt{c_1^2 - y_1^2}\, \alpha y_1}{|\alpha y_1|}, \tag{13}$$

$$d = \sqrt{x_1^2 + y_1^2} + \frac{1}{2}l, \tag{14}$$

$$a_{max} = d\sqrt{\alpha^2 + \omega^4}, \tag{15}$$

where c_2 – distance between the minimum magnitude point of the total acceleration field and the solenoidal vector field center; c_1 – distance between the minimum magnitude point of the total acceleration field and the converging vector field center; y_1 – offset of the total acceleration vector field center along y-axis; x_1 – offset of the total acceleration vector field center along the x-axis; d – distance from the farthest point within the CA to the center of the total acceleration vector field.

If the UGV CA is not horizontal, effects of gravitational acceleration must be taken into account. For simple UGVs, terrain angle mostly defines the orientation of its frame in relation to the gravitational acceleration field. More sophisticated UGVs have a capability to change the orientation of the CA in relation to terrain. In both cases, the inclination of the CA requires narrowing the limits of acceleration to cope with the gravitational acceleration. Digital maps that have terrain angle information can be divided into more and less safe areas for safe trajectory planning. Driving on unmapped terrain requires the reduction of tangential motion parameter limits in real time.

The following formulas can be used to find the additional shifting of the minimum magnitude point of the total acceleration vector field:

$$x_2 = \frac{a_x}{\omega^2} - \frac{\left(\dfrac{a_y}{\alpha} + \dfrac{a_y}{\omega^2}\right)\alpha^2}{\alpha^2 + \omega^4}, \tag{16}$$

$$y_2 = \frac{a_y}{\omega^2} + \frac{\left(\dfrac{a_x}{\alpha} - \dfrac{a_y}{\omega^2}\right)\alpha^2}{\alpha^2 + \omega^4}, \tag{17}$$

$$d = \sqrt{(x_1 + x_2)^2 + (y_1 + y_2)^2} + \frac{1}{2}l, \qquad (18)$$

where x_2, y_2 – additional shifting of the acceleration vector field's minimum magnitude point along the x and y-axis; a_x, a_y – gravitational acceleration along the x and y-axis.

In the non-symmetric drive mode the effects of gravitational acceleration cause the minimum magnitude point to move (Figure 44). The following schematic illustrates the additional shifting:

Figure 44. Shifting of the minimum magnitude point on slopes

4.7 Proportional Velocity Command Reduction

Because maximum acceleration in the CA is a function of four parameters (v_L, v_R, a_L, a_R assuming track width $l = 1$ remains constant), it is difficult to visualize all effects of all four input variables in one printable plot. Two worst case acceleration

combinations have been picked to find the most restricting cases to the safe input velocity combination sets illustrated in Figure 45a-b and Figure 46a-b.

(a)

(b)
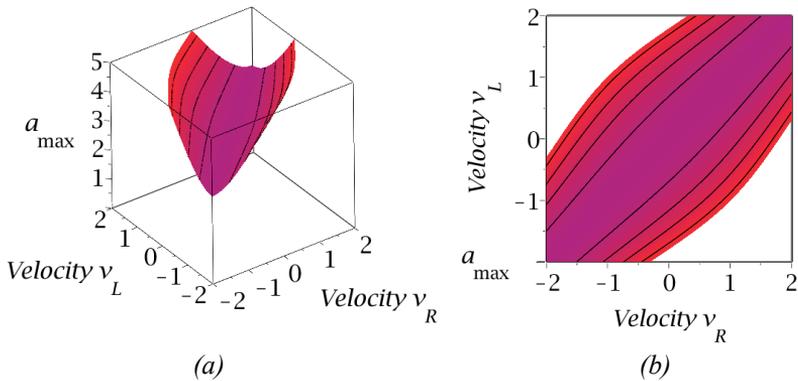
Figure 45. Maximum acceleration surface plot (a_L=3 m/s^2, a_R=3 m/s^2): (a) normal view; (b) top view

(a)

(b)
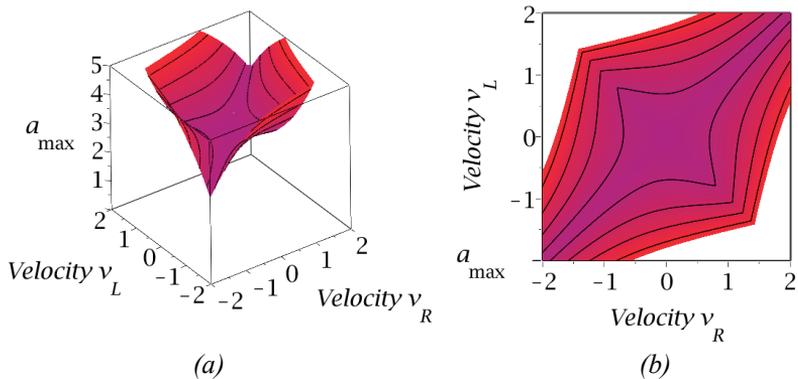
Figure 46. Maximum acceleration surface plot (a_L=−3 m/s^2, a_R=3 m/s^2): (a) normal view; (b) top view

Plots have been cropped to (a_{limit} = 5 m/s^2) to clearly distinguish between the sets of allowed and disallowed velocity combinations. Any velocity combination must be presented in both of the allowed sets (presented in color) not to cause maximum acceleration magnitude above a_{limit} while tangential accelerations of the left and right side reference points may vary between −a_{lim} to a_{lim}.

Proportional Velocity Command Reduction (PVCR) suppresses left and right side velocity commands proportionally to retain original turn radius. The coefficient of reduction b must always be applied to both of the tangential velocity commands ($v_{Lm} = v_L b$ and $v_{Rm} = v_R b$), not to change the original ratio of tangential velocities. Thus, in case the reduction is not necessary, the coefficient defaults to 1, otherwise $0 < b < 1$.

Default tangential velocity limits of AMPP allow no tangential velocity combinations outside a combination set of: −2 ≤ v_L ≤ 2 and −2 ≤ v_R ≤ 2. Skewed

ellipse (Figure 47) has been chosen to describe the perimeter of the combination set within that square outside of which PVCR should be used for moving velocity combinations in the command space to the safe combination set perimeter.

If the maximum acceleration magnitude limit is set to 5 m/s^2, the following condition must be met for satisfying the criteria for safe drive:

$$a_{limit} \geq \frac{-3v_L v_R + 2v_L^2 + 2v_R^2}{l_1}, \tag{19}$$

where a_{limit} – maximum acceleration magnitude limit; l_1 – distance 1 m;
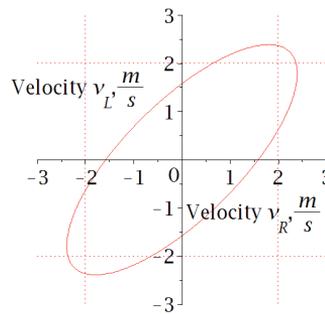
Figure 47. Threshold of the safe velocity combination set (a_{limit} = 5 m/s^2)

The coefficient of velocity command reduction is calculated by the formula:

$$\begin{cases} b = 1, & \text{if} \quad \dfrac{-3v_L v_R + 2v_L^2 + 2v_R^2}{l_1} \leq a_{limit} \\[4mm] b = \sqrt{\dfrac{a_{limit} l_1}{-3v_L v_R + 2v_L^2 + 2v_R^2}}, & \text{if} \quad \dfrac{-3v_L v_R + 2v_L^2 + 2v_R^2}{l_1} > a_{limit}, \end{cases} \tag{20}$$

where b – velocity reduction coefficient.

The coefficient b, when applied to the original velocity commands, suppresses velocity commands just enough to bring the velocity combination from disallowed combination set to the perimeter of the described ellipse.

Isolines of Figure 45 and 46 suggest that maximum acceleration limits below 5 m/s^2 may require separate formulas for changing velocity combinations at symmetric and anti-symmetric tangential acceleration extremities.

4.8 AMPP-fitted Proportional Velocity Command Reduction

Simulation results show that the suppression method previously described is much too strict for AMPP input processing because AMPP gradually decreases tangential

acceleration as the tangential velocity approaches its upper (v_{lim}) or lower ($-v_{lim}$) limit. A more suitable surface plot that allows finding safe velocity combination sets is presented in Figure 48a-b.

(a)   (b)
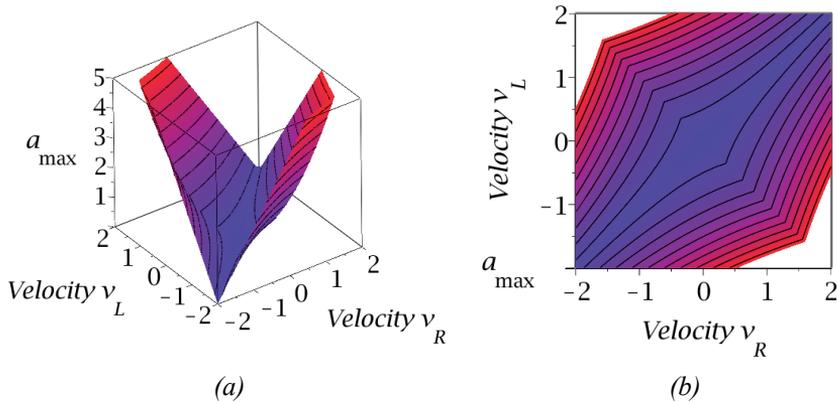
Figure 48. Maximum acceleration surface plot (a_L=0 m/s^2, a_R=0 m/s^2): (a) normal view; (b) top view

Perimeter of the allowed set of velocity combinations that have total acceleration magnitude limit (a_{limit}) at 5 m/s^2 is described in Figure 49. Tangential velocity combination set is otherwise defined only by the default tangential velocity limits (-2 m/s to 2 m/s).
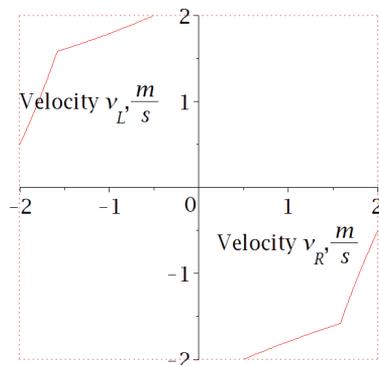
Figure 49. AMPP-optimized safe velocity combination set threshold (a_{limit} = 5 m/s^2)

Suitable velocity reduction coefficient b can be calculated by:

$$\begin{cases} b = 1, & \text{if} \quad \frac{1}{2l}\left[\left|v_R{}^2 - v_L{}^2\right| + \left(v_R - v_L\right)^2\right] \leq a_{limit} \\ b = \sqrt{\dfrac{2la_{limit}}{\left|v_R{}^2 - v_L{}^2\right| + \left(v_R - v_L\right)^2}}, & \text{if} \quad \frac{1}{2l}\left[\left|v_R{}^2 - v_L{}^2\right| + \left(v_R - v_L\right)^2\right] > a_{limit} \end{cases}$$

(21)

56

AMPP-fitted PVCR was implemented by the following Simulink diagram (Figure 50). S-function (labeled "c_t") calculates the variable *b*. Velocity command reduction can be disabled by changing the "Mode" gain to zero. 3DScope component [39] was used for simultaneous visualization of the modified velocity commands and actual velocities of the left and right side assuming the commands are performed perfectly by AMPP blocks of each side.
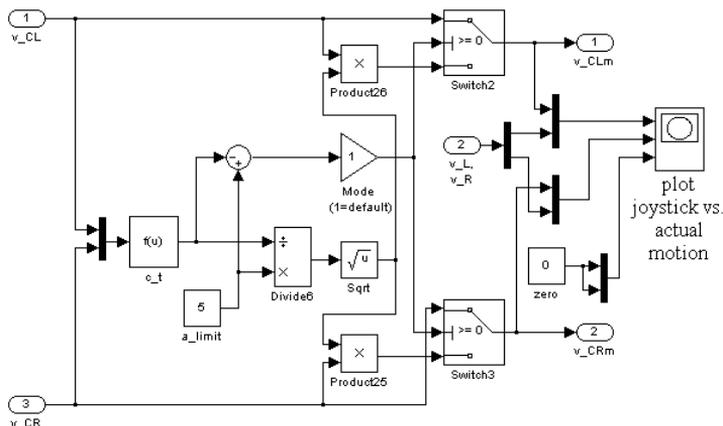
Figure 50. Simulink diagram of PVCR

4.9 Simulation of AMPP-fitted PVCR

To test the effectiveness of PVCR, sequences of the worst case input velocity command were created (Figure 51 and 52).
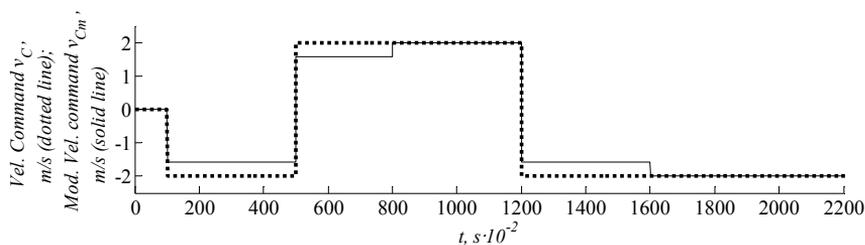
Figure 51. Input velocity command modification (PVCR) plot of the left side
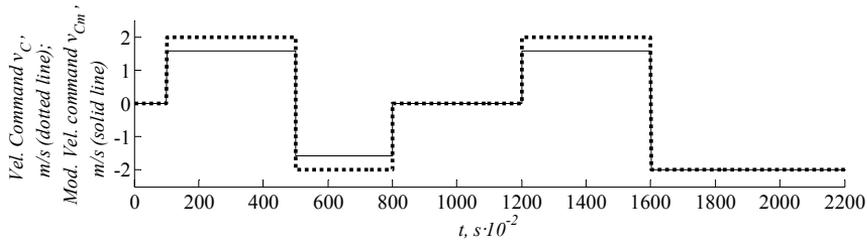
Figure 52. Input velocity command modification (PVCR) plot of the right side

The same plots demonstrate how velocity commands are being modified. As can be seen, at the 8th second, decreasing one side velocity allows slightly higher velocity to be used at the opposite side and it disables the input velocity command modification. Without PVCR enabled, the maximum acceleration comes close to 8 m/s^2, as seen in Figure 53.
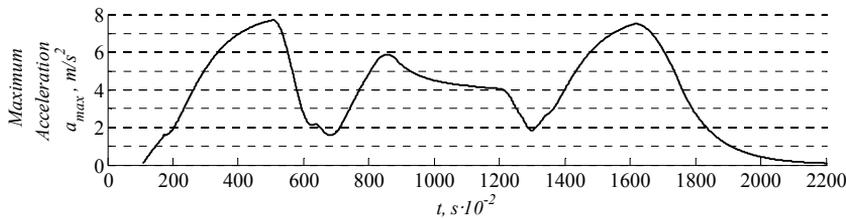
Figure 53. Maximum acceleration magnitude in the CA without PVCR

Maximum acceleration limit 5 m/s^2 from previous examples was chosen for the PVCR limit. Figure 54 demonstrates how PVCR limits maximum acceleration effectively except shortly after the 16th second, where noticeable violation occurs. This exception happens when the UGV exits maximum velocity zero-radius turn by intensely braking one side. The Command Pre-Processor, further described in the following chapters, solves that problem with insignificant restrictions to the UGV maneuverability.
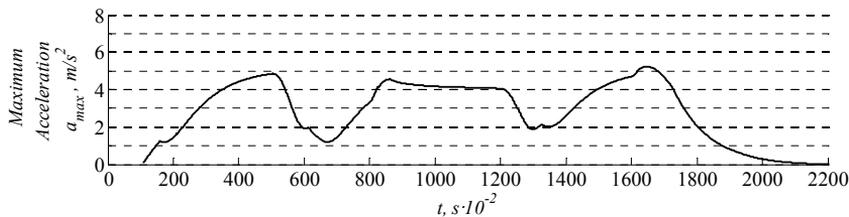
Figure 54. Maximum acceleration magnitude in the CA with PVCR

4.10 User interface for the creation of input velocity commands

Conventional 2-axis joystick fits well for an input velocity command device if it is rotated counter clockwise $\pi/4$ radians because its x and y axes may be easily

translated to the velocities of the left and right side reference point. A user can control the vehicle to drive straight by pushing the joystick forward. Joystick with a square gate does not limit any combination of *x* and *y* outputs. Joysticks with octagon and circular gates may cause unnecessary velocity combination restrictions.

Figure 55 demonstrates how UGV's turning radius can be kept by gradually moving the joystick along one of the dotted lines up to the centermost position.
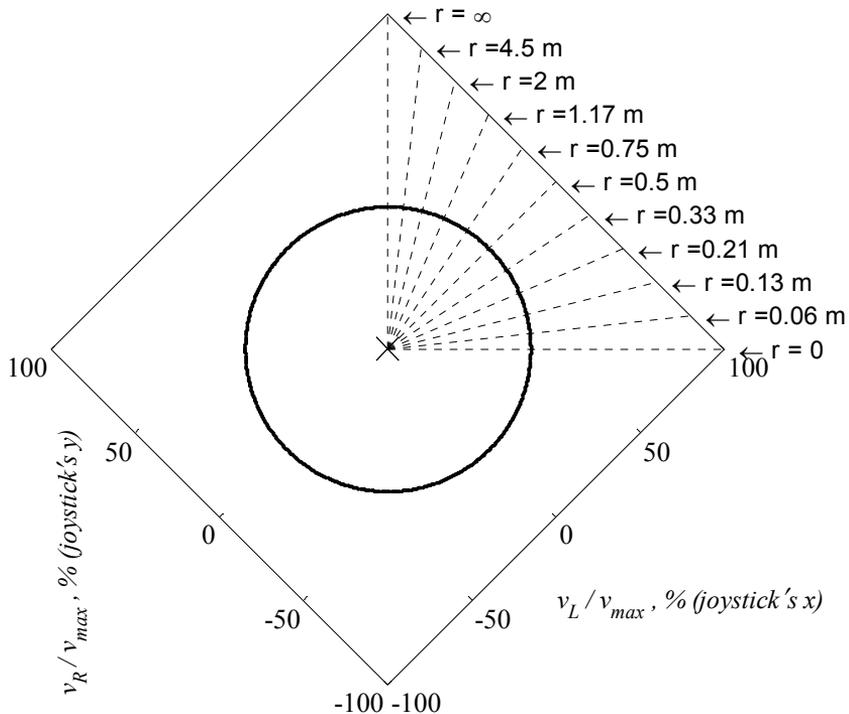
Figure 55. Joystick area with equal turn radius (dotted) lines

If the velocity command set is only limited in software, the UGV operator receives no direct tactile feedback from the joystick when entering or leaving the safe area. Many modern joysticks have a FFB (Force Feedback) capability. Energized coils inside FFB joysticks can be used for affecting joystick movement, depending on the shape and size of a safe command space. If FFB coils are energized and switched off at the threshold of a safe contour, it is physically quite effortless for the UGV operator to perceive the size and shape of the window of the safe area by tactile sensing. Most of the time the UGV operator is expected to work in the safe area. However, with minor changes to the control software, it is possible to add an override capability. So by holding down specific buttons, soft gates can be changed or completely disabled for some less common maneuvering.

4.11 Command Pre-Processor

Simulations show that when anti-symmetric motion (maximum angular velocity) is instantly switched to symmetric motion, tangential accelerations of the left and right side reference point cannot be disregarded. In this particular case, maximum acceleration violates a_{limit} for a short period. One possible solution to overcome this problem is to exclude certain velocity combinations by some additions to the Command Pre-Processor.

Figure 56 presents the joystick movement area with corresponding turning radiuses. In the default mode, all velocity combinations are allowed.
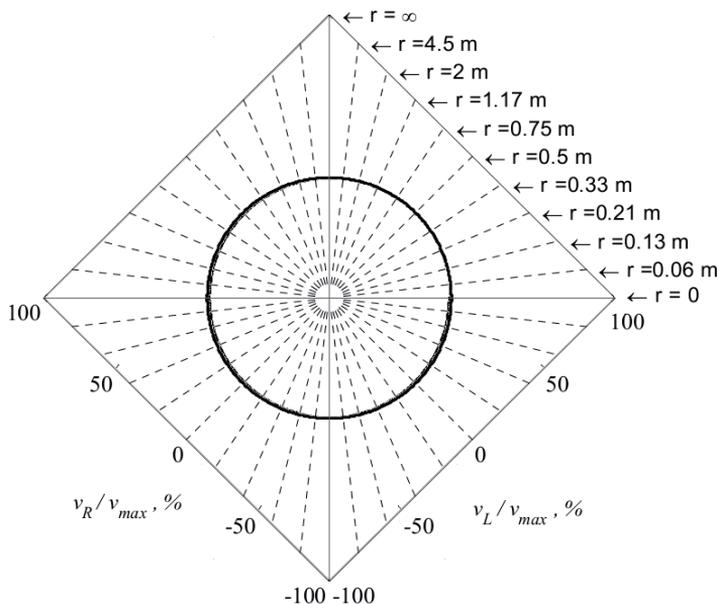
Figure 56. All velocity combinations (and turn radiuses) allowed

In everyday use, very small radius turns are not very useful. STRA (Small Turning Radius Avoidance) in Figure 58 excludes certain velocity command combinations from the command space, without eliminating indispensable zero-radius turning capability.
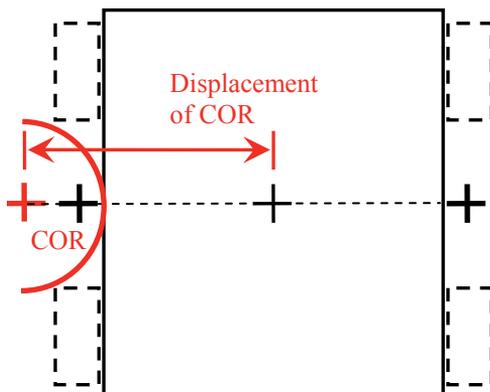
Figure 57. Minimum useful displacement of COR for normal turning (red)

Figure 57 demonstrates how minimum useful displacement of the center of turning the radius is related to the geometry of a vehicle. Minimum clearance threshold has been marked with a red arc. If UGV wheels are covered by the UGV frame, minimum useful displacement of COR would still be half the track width or more. It is safe to assume that for normal turning, radiuses below ½ of the track width do not contribute to better maneuverability by allowing sharper turns around trees or poles.
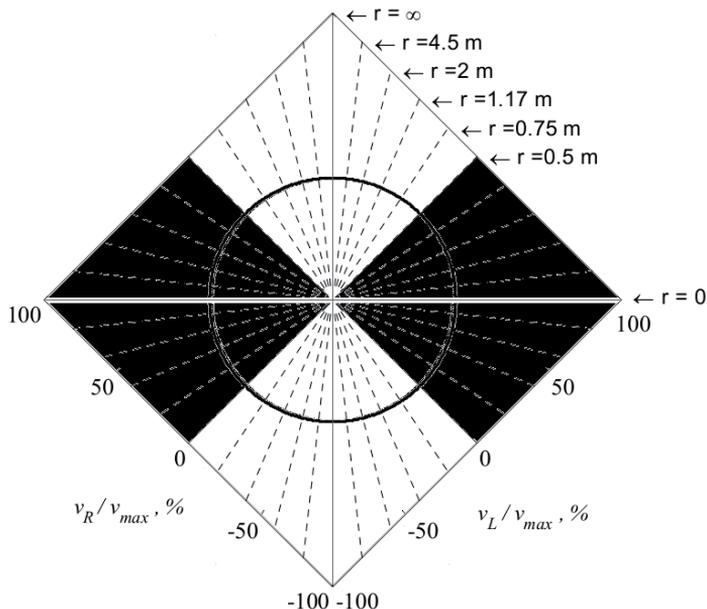
Figure 58. STRA mode (disabled velocity combinations as black area)

Normal drive combination sets (white squares in Figure 58) and zero-radius overlap near zero, so either one of the combination sets can be freely entered from

complete stop. Exclusion of velocity combination depends on the actual UGV motion and inhibits the UGV operator to skip over the excluded velocity combination sets. For increased safety, zero radius turn may be activated only by added fail-safe, like holding down a dedicated button at zero velocity.

Joystick is one of many human interface input devices, which can be used for creating input velocity commands in real-time. Still, for better perception of the controllability of the virtual UGV model, actual joystick input was used as an input velocity command device. One two-axis (one-joystick mode) and two one-axis joysticks (two-joystick mode) were tested with MP. A mode can be selected by changing the value of "joystick mode" to one or zero in Figure 59. Two-joystick mode was more convenient as moving one joystick did not unintentionally move the other. Having one joystick for throttle and another for steering is also a common setup for remotely controlled ground vehicles. Rotating joystick axes was made virtually. Dead zone, gain and saturation were introduced for general purpose joystick adjustments. Red highlighted parts of the schematic represent STRA and TBB (Turn By Braking) functionality. "Switch5" to "Switch8" have thresholds of –0.1 m/s, allowing overlap of normal drive mode and zero radius turn mode near zero. Safety button functionality for zero radius turns was not implemented.
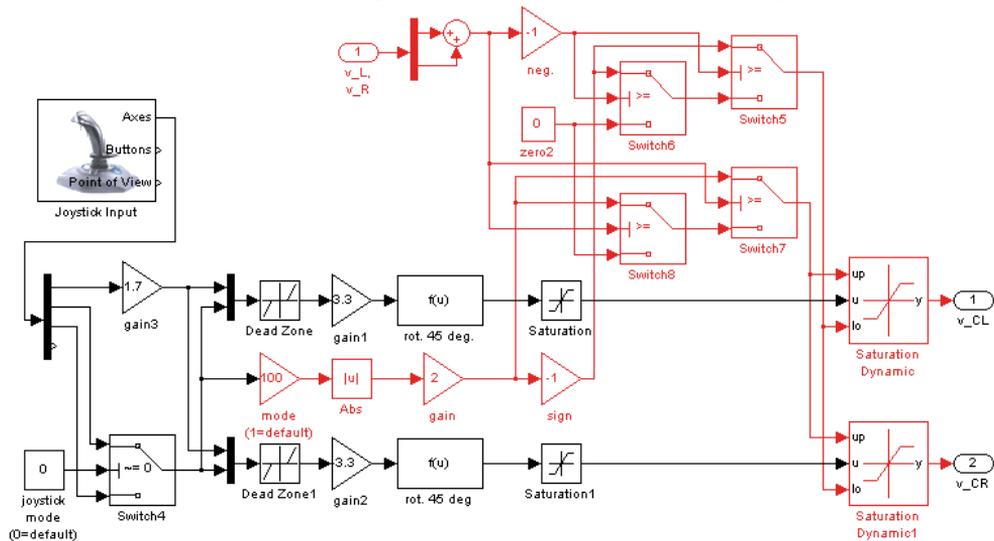
Figure 59. Joystick input subsystem

Figure 60a-b demonstrate how STRA is much stricter than an unprocessed command space. Both demonstrate also the usage of PVCR.
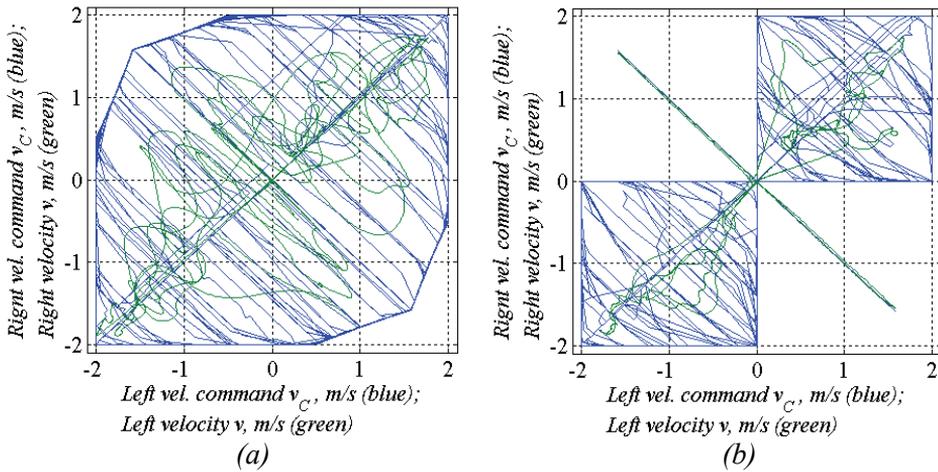
Figure 60. Command Pre-Processor STRA evaluation plots: *(a) PVCR*; *(b) PVCR with STRA*

In case the UGV is driving straight, both reference points at their maximum tangential velocity entering a curve may be done only by reducing one side velocity. The same situation at lower velocities is different as the opposite side can also increase its velocity. Such inconsistency may be disturbing for the UGV operator. Turn by braking (the right plot in Figure 61) solves this problem with dynamic saturation. The *y*-axis of a joystick determines the level of saturation and the *x*-axis of a joystick determines the difference of the left and right side velocities. When joystick axes have been assigned to physically separated joysticks (joystick mode 0), it is convenient to keep a steady pace with one thumb and adjust turning radius with another.
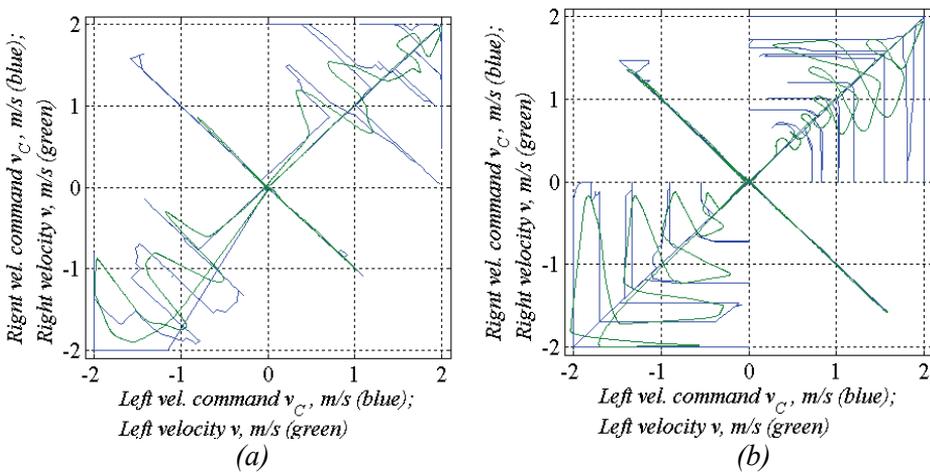
Figure 61. Command Pre-Processor TBB evaluation plots: *(a) PVCR with STRA*; *(b) PVCR, STRA and TBB on the right*

Velocity commands and actual velocities have been created mostly by moving the *y*-axis in steps. At every step the *x*-axis was moved both ways. Zero-radius turning was done differently. Firstly, the *x*-axis of a joystick was moved to its maximum, and then the throttle (*y*-axis) was carefully increased.

STRA with TBB is more convenient for the UGV control than other presented modes, and it perfectly eliminates maximum acceleration peak exception.

Figure 62 describes one possible way to distribute all proposed control modules between the Control Station and on-board electronics of the UGV.

4.12 Overview of the proposed methods

Figure 62 describes a possible architecture of the proposed control modules for the UGV control and the main data connections between them. Modules have been distributed into two main groups: the Control Station and the vehicle. If a 2-axis input device has FFB capability, it can be used for informing the UGV operator about the safe command space for currently selected motion parameter limits. Because FFB data do not depend on the actual motion of the UGV, there is no interference to the motion of a 2-axis input device. Neither is there a need for transmitting FFB related data from the UGV to the Control Station. The command space of allowed velocity combinations depends on the Command Pre-Processor modules and their settings.

Main wireless data stream between the Control Station and the UGV contains mostly velocity commands and some rare motion parameter limit changes. AMPP modules use real-time motion feedback to make short motion simulations to find the most suitable output command for each time-step. If an obstacle is detected on the path of the UGV, the distance to the obstacle is used for automatic stopping.
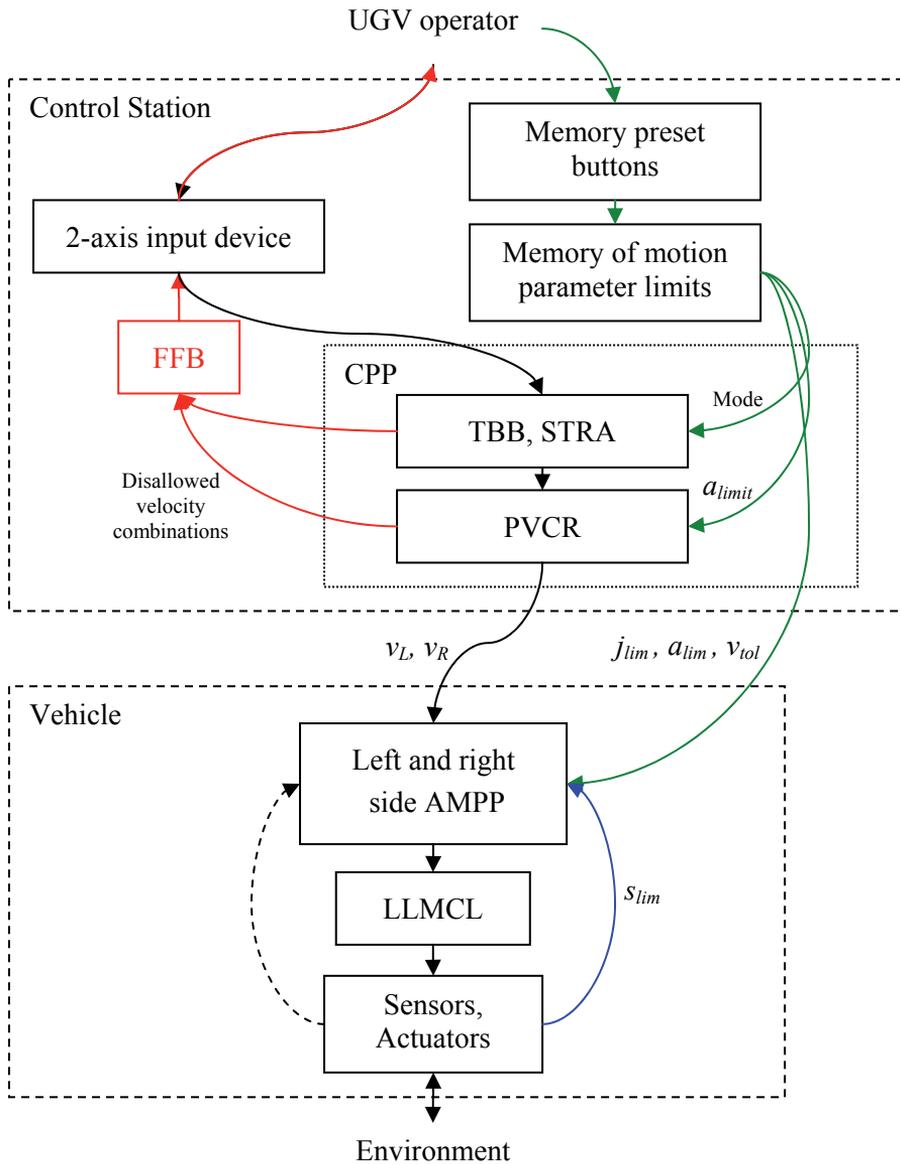
*Figure 62. Data flow diagram (motion parameter limits – green; motion commands –
black; motion feedback – black dotted; data for tactile feedback – red; obstacle distance –
blue)*

Several routine parameter and control mode choices must be made by the UGV
operator prior to controlling the vehicle motion by the 2-axis input device. For each
option, there are some guidelines, as shown in Figure 63. Settings of control
modules can be optimized for particular types of tasks. Memory presets help the
UGV operator to keep the settings organized and activate them quickly, for

example, by pressing on the memory preset buttons on the panel of the Control Station.

Action   Guideline

```
┌─────────────────────┐                      ┌─────────────────────┐
│ Choose limits for   │                      │ Mostly UGV          │
│ tangential motion   │ ─ ─ ─ ─ ─ ─ ─ ─ ─ ─► │ capabilities and    │
│ parameters or use   │                      │ servo ratings       │
│ memory preset       │                      │ (impact resistance) │
└─────────────────────┘                      └─────────────────────┘
           │
           ▼
┌─────────────────────┐                      ┌─────────────────────┐
│ Set suitable radius │                      │ Placement of        │
│ for the CA or use   │ ─ ─ ─ ─ ─ ─ ─ ─ ─ ─► │ acceleration-       │
│ memory preset       │                      │ sensitive on-board  │
│                     │                      │ equipment           │
└─────────────────────┘                      └─────────────────────┘
           │
           ▼
┌─────────────────────┐                      ┌─────────────────────┐
│ Choose maximum      │                      │                     │
│ acceleration        │                      │ Ratings of jerk and │
│ magnitude limit or  │ ─ ─ ─ ─ ─ ─ ─ ─ ─ ─► │ acceleration-       │
│ use memory preset   │                      │ sensitive equipment │
└─────────────────────┘                      └─────────────────────┘
           │
           ▼
┌─────────────────────┐                      ┌─────────────────────┐
│ Choose operating    │                      │ Experience level    │
│ modes (TBB, Mode B) │ ─ ─ ─ ─ ─ ─ ─ ─ ─ ─► │ and preferences of  │
│ or use memory preset│                      │ the UGV operator    │
└─────────────────────┘                      └─────────────────────┘
           │
           ▼
┌─────────────────────┐                      ┌─────────────────────┐
│ Choose target       │                      │ Priority of         │
│ velocity tolerance  │ ─ ─ ─ ─ ─ ─ ─ ─ ─ ─► │ velocity precision  │
│ or use memory preset│                      │ or energy efficiency│
└─────────────────────┘                      └─────────────────────┘
           │
           ▼
┌─────────────────────┐                      ┌─────────────────────┐
│ Start sending       │                      │                     │
│ velocity commands   │ ─ ─ ─ ─ ─ ─ ─ ─ ─ ─► │ Task                │
│ with 2-axis input   │                      │                     │
│ device              │                      │                     │
└─────────────────────┘                      └─────────────────────┘
           │
           ▼
┌─────────────────────┐                      ┌─────────────────────┐
│ Set automatic       │                      │                     │
│ stopping point      │                      │ Distance to an      │
│ (manually or        │ ─ ─ ─ ─ ─ ─ ─ ─ ─ ─► │ obstacle or docking │
│ automatically by    │                      │ station             │
│ obstacle sensor     │                      │                     │
│ data)               │                      │                     │
└─────────────────────┘                      └─────────────────────┘
```

Figure 63. UGV operator's routine choices and preparation guidelines

4.13 Chapter summary

- Methods for the curvilinear motion control of the UGV, which keep the maximum acceleration magnitude within prescribed limits, were proposed in this section of the thesis.
- Further development of MP algorithms may combine smooth control of the vehicle with obstacle avoidance by automatically switching to alternative smooth trajectories of the UGV.
- Jagged and narrow paths require that the UGV reduces velocity not to exceed the limits for motion parameters.
- Entire acceleration vector field within the CA can be indirectly measured by two accelerometers at the left and right reference point of the UGV.
- Vector fields of different origin (caused by centripetal acceleration and tangential acceleration of reference points) may have a minimum magnitude point shifted along the x-axis of the UGV coordinate system.
- Minimum magnitude point of the total acceleration field may be shifted along both axes.
- The magnitude of the total acceleration field increases linearly with the distance from the minimum magnitude point.
- Joysticks with FFB can be used for tactile feedback about the extent of the excluded velocity combination set.
- PVCR with Mode B keeps the maximum acceleration magnitude within limits in any velocity input.
- TBB makes the UGV response to manual control more consistent.
- Cost function for optimal path planning can be made by time alone as rough terrain necessitates decreasing the UGV velocity.

5. LOCAL TRAJECTORY PLANNING

5.1 Tracking the reference path

Tracking mode is a semi-autonomous control mode, which does not have the maneuverability of conventional control mode, but it may be useful if the UGV operator needs to focus on other tasks than steering the vehicle.

Tracking and obstacle avoidance can be implemented with an additional high level motion control module. TC (Turn Coordinator) shown in Figure 64 simulates a set of alternative trajectories (a.k.a. virtual tentacles) and alters velocity command input to coordinate the turns by the best fitting virtual tentacle.

User Input

| TC |
| CPP |
| Left and right side AMPP |

LLMCL
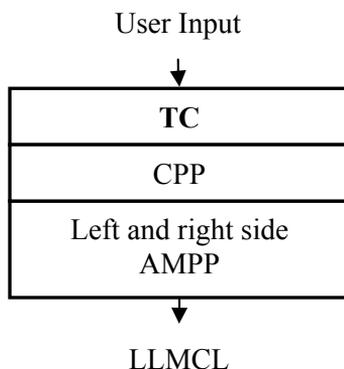
Figure 64. Turn Coordinator added to the layered approach of the UGV control

Virtual tentacles are created in the TC module by separate motion simulations, which use the same motion parameter limits as other control modules but the processing is made separately. It switches either side velocity command to a zero value for a certain amount of time-steps to make the necessary turns (Figure 65).
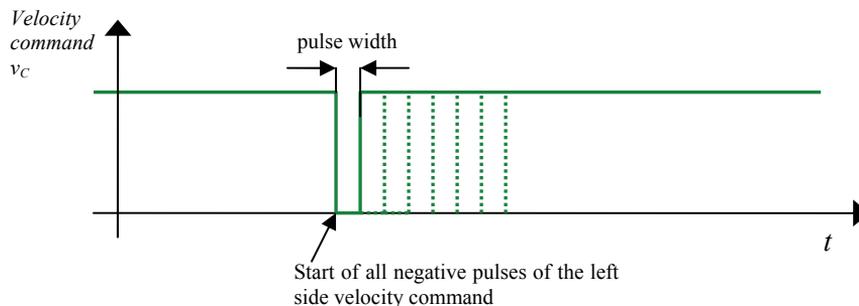
Figure 65. Using negative velocity command pulses for creating tentacles

Data about obstacles must be sent to TC to find a route around them. If none of the virtual tentacles fit to the virtual map of obstacles, TC initiates the automatic stopping mode by setting target velocity to zero.

Arithmetic mean value of the left and right velocity command is used for TC input (left and right side tangential velocity command). The UGV operator can stop or slow down the vehicle at any time by setting velocity commands to a lower level or zero.

Motion analysis was made to visualize the shape and distribution of virtual tentacles. Every tentacle was created within 10 s of separate motion simulation. All tentacles represent trajectories, which the UGV can safely track, without the necessity for significant overall velocity reduction. The first tentacle is a straight reference line and does not use one side braking. The first negative pulse has the duration of one time-step (0.01 s). The following 24 tentacles in Figure 66 were created with progressively longer negative pulse widths up to the longest (2.33 s).
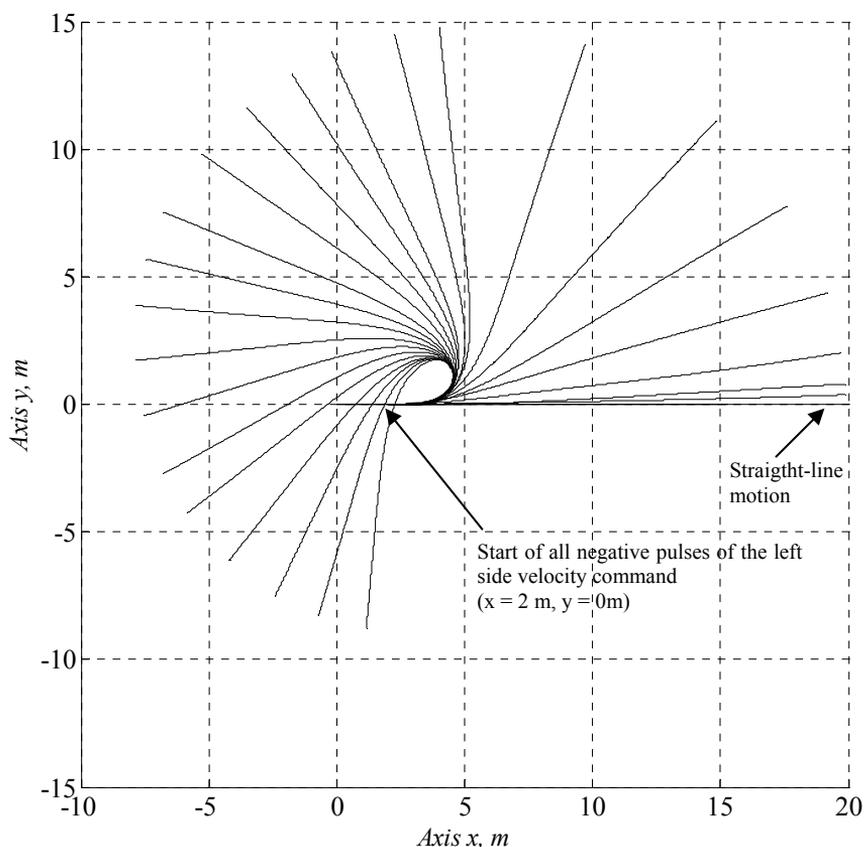
Figure 66. Trajectories created by the left side velocity command pulse timing with the default motion parameter limits

All negative pulses were introduced after 1 s of driving at 2.0 m/s, starting from the zero point of both axes.

To visualize how the reduction of a_{limit} changes tentacle shapes, another motion analysis was made with a_{limit} set to 3.1 m/s^2, shown in Figure 67. The shape and distribution of tentacles allows creating safe trajectories by simple negative pulses of either side velocity command.
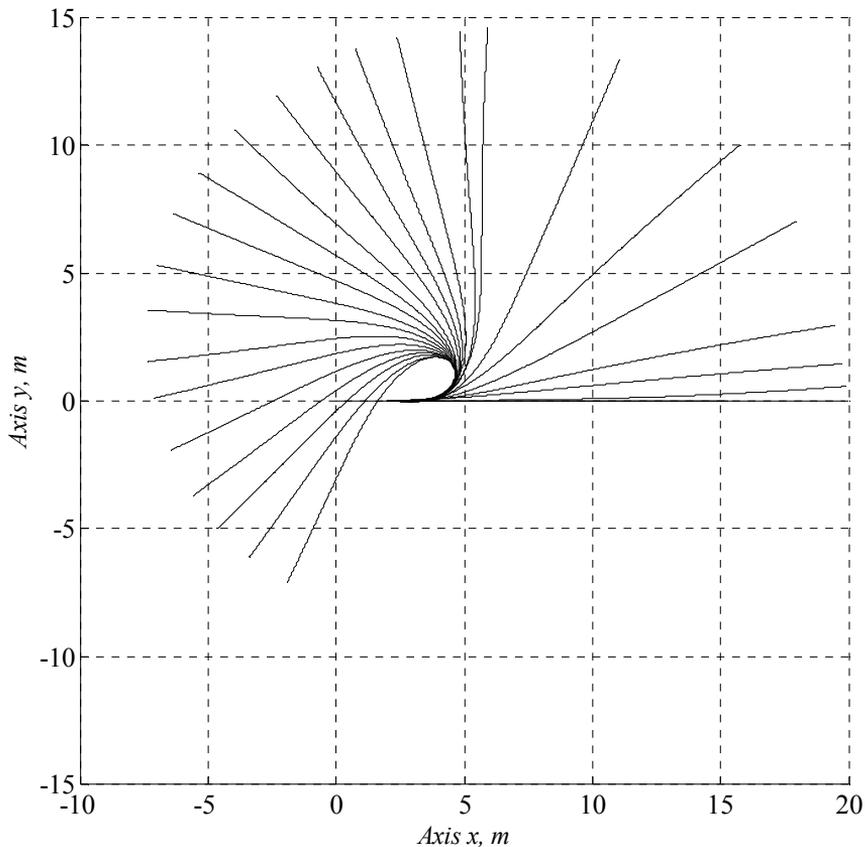
Figure 67. Trajectories created by the left side velocity command pulse timing with the default motion parameter limits except a_{limit}

5.2 Chapter summary

- Possible local path planning method was analyzed in this section.
- TC must have data about obstacles and a reference path to find the best fitting alternative and safe trajectories for the UGV motion.
- Tracking mode allows stopping the vehicle at any time but it lacks maneuverability.

CONCLUSIONS

This thesis focuses on solving the skid-steer UGV control problems like residual vibrations (rocking of the vehicle), current surges, human error (collisions, flip-over) and impact to the UGV system and loading by adding high level control modules to the UGV control system. Methods for using in the UGV control system have been elaborated step-by-step as new shortcomings have been brought up by motion simulations and analyses.

Main conclusions

- The presented thesis proposes a novel approach to the skid-steer UGV control. In contrast to the conventional motion and trajectory planning methods of UGVs, which mainly focus on the environment, this study mainly focuses on the safety-critical motion of the UGV system and loading.
- AMPP modules effectively limit jerk, acceleration, velocity and distance of tangential motion of the left and right side reference points.
- PVCR was added to CPP to exclude unsafe velocity combinations and to reduce the velocity of the left and right side proportionally to maintain the original turning radius.
- STRA module solved the problem of acceleration magnitude violation exception when the UGV spiraled out of the zero-radius turn.
- TBB module made UGV control more consistent at high velocities.
- Motion analysis and motion simulation results prove the presented concepts to be useful for the skid-steer UGV control.
- Simulation results suggest MP concepts to be useful also in applications where reference path tracking and obstacle avoidance are required.

Main contributions

- Novel skid-steering UGV control method was developed to reduce impact on the UGV system, safety-critical loading and to reduce residual vibrations.
- Method of using novel Active Motion Profile Planners and a Command Pre-Processor for the skid-steer UGV control was developed to keep critical motion parameters within their limits while allowing maximum controllability by the user input.
- Virtual models for testing the effectiveness of the proposed concepts were developed.

Future work

Methods of the UGV control proposed in the thesis could be evaluated and further developed by real life experimentation with the universal UGV prototype. This UGV was developed and built in a research project that was originally not focused on the safe motion of the UGV CA [1]. Wheels at the end of each motorized leg enable reducing UGV clearance up to zero and also raising the clearance to maximum for the least energy-consuming zero-radius turns. By changing the stance of the UGV, also climbing up and down the terrain slopes can be made more efficient, as different stances influence the UGV weight distribution on wheels.

New concepts for changing the stance and CA inclination automatically would contribute to keeping the motion of the CA within safe limits. The UGV and terrain-specific problems such as wheel slippage, flip-off prevention and 3-wheel drive modes could be investigated to make the UGV motion safer for off-road use as well.

Enhanced obstacle avoidance, instead of just stopping before colliding with it, would be useful in some future semi-autonomous or fully autonomous operating modes. Capability of making a few more numeric simulations per time-step to assess different safe trajectories (virtual tentacles) and choose the best fitting one is not a simple task but it may be profitable to develop. To keep the number and selection of virtual tentacles optimal, ideas from many other studies could be adopted to the proposed concepts.

As far as critical motion of the CA is concerned, the trajectories created in Figure 68a-b have obvious jaggedness, which take a toll of either high acceleration and jerk peaks or long travel time.

(a)   *(b)*
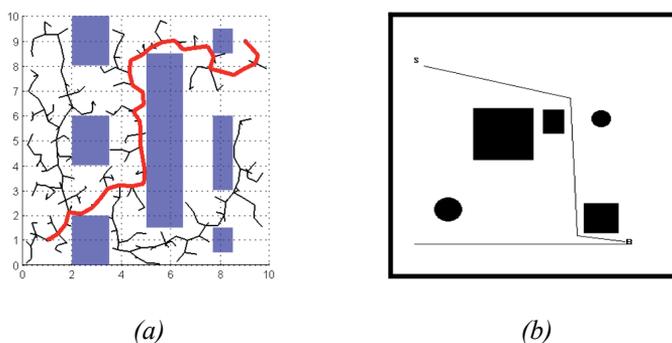
Figure 68. Examples of trajectories: (a) using rapidly exploring random tree for path planning [40]; *(b) intelligent path planning with sharp (zero-radius) turns* [41]

Jagged paths could be processed to provide alternative trajectories with large and gradually changing radiuses, so UGVs can follow these trajectories at steady pace without causing high acceleration and jerk peaks within the CA.

Some studies solve path finding problems by digital maps created from the data of digital aero-photos (Figure 69).
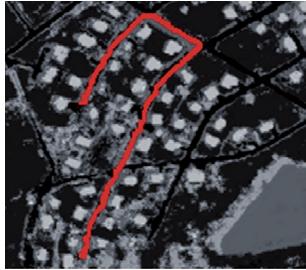
Figure 69. Path planning based on aero photos [42]

In urban areas, there are often tarmac, grass, sand or gravel surfaces to choose from. Different roughness classes, which are visually distinguishable, help to evaluate options of path placement automatically. Cost functions and cost maps can be made with different priorities in mind. For example, in [42] the cost functions consider mostly time and energy needed by an UGV to drive a certain length of a particular terrain class.

New methods of path evaluation would consider not only the terrain properties but also the width and jaggedness of the path. Taking small radius turns often requires velocity reduction and, in most cases, consumes more time and energy.

PointCom is an intuitive semi-autonomous control interface for the UGV control, which is inspired from the concepts used in modern strategy gaming [43]. The UGV operator can click at the next destination of the UGV on a 3D map, without having to deal with exact trajectory picking and setting up automatic stopping points. Tentacle-based reference path tracking method could be combined with a reference path generator, which connects all inserted positions into a reference path to obtain an alternative control method with a capability to automatically drive around certain obstacles, while also tracking the main reference path.

If many unmanned vehicles share data about their planned trajectories, terrain properties and detected obstacles, coordination of included vehicles could be made more efficiently.

Next steps of the study
- To develop an on-board digital map, reference path tracking and obstacle avoidance capability based on MP concepts
- To develop long-range trajectory planning capability and fully autonomous driving mode based on MP concepts
- To develop an automatic information sharing coordination system for a number of ground and aerial vehicles

REFERENCES

1. Mandow, A., Martínez, J. Experimental kinematics for wheeled skid-steer mobile robots. ― *IEEE/RSJ International Conference on Intelligent Robots and Systems 2007, IROS 2007*. 2007, 1222–1227

2. Fourlas, G. K. Fault detection approach for a 4 - wheel skid steering mobile robot. ― *IEEE International Conference on Industrial Technology 2013, ICIT*. IEEE, 2013, 64–68

3. Yi, J., Song, D., Zhang, J., Goodwin, Z. Adaptive trajectory tracking control of skid-steered mobile robots. ― *IEEE International Conference on Robotics and Automation 2007*. 2007, (04), 10–14

4. Pazderski, D. Practical stabilization of a Skid-steering Mobile Robot - A Kinematic-based Approach. ― *Proceedings of the Fourth International Workshop on Robot Motion and Control 2004, RoMoCo'04*. 2004, 519–524

5. Yu, W., Chuy, O. Dynamic modeling of a skid-steered wheeled vehicle with experimental verification. ― *International Conference on Intelligent Robots and Systems 2009, IROS 2009*. 2009, 4212–4219

6. Zweiri, Y. H., Seneviratne, L. D., Althoefer, K. Non-linear observer for slip estimation of skid-steering vehicles. ― *Proceedings of IEEE International Conference on Robotics and Automation 2006, ICRA*. IEEE, 2006, (05), 1499–1504

7. Jian, Z., Shuang-shuang, W., Hua, L., Bin, L. The sliding mode control based on extended state observer for skid steering of 4-wheel-drive electric vehicle. ― *2nd International Conference on Consumer Electronics, Communications and Networks 2012, CECNet*. IEEE, 2012, 2 2195–2200

8. Lhomme-Desages, D. Trajectory control of a four-wheel skid-steering vehicle over soft terrain using a physical interaction model. ― *IEEE International Conference on Robotics and Automation 2007*. 2007, (04), 10–14

9. Shuang, G., Cheung, N. Skid Steering in 4-Wheel-Drive Electric Vehicle. ― *7th International Conference on Power Electronics and Drive Systems 2007, PEDS '07*. 2007, 1548–1553

10. LBC - Little Benthic Crawler [WWW] http://www.seabotix.com/products/lbc.htm (25.05.2013)

11.   Micro UGV To Neutralize IEDs [WWW] http://www.hightech-edge.com/micro-ugv-to-neutralize-ieds/8404/ (25.05.2013)

12.   Autonomous and Remote Control Ground Vehicle at Centre of Marshall Involvement in National Science Week [WWW] http://www.marontech.co.uk/autonomous-and-remote-control-ground-vehicle-at-centre-of-marshall-involvement-in-national-science-week (25.05.2013)

13.   Allen Vanguard To Distribute Unmanned Ground Vehicles (UGV) [WWW] http://www.unmanned.co.uk/unmanned-vehicles-news/unmanned-ground-vehicles-ugv-news/allen-vanguard-to-distribute-unmanned-ground-vehicles-ugv/ (25.05.2013)

14.   COBRA MK2 - Mini UGV for inspection in confined areas [WWW] http://www.eca-robotics.com/en/robotic-vehicle/robotics-terrestrial-unmanned-ground-vehicles-(ugv)-cobra-mk2-mini-ugv-for-inspection-in-confined-areas/26.htm (25.05.2013)

15.   Vegetation Classification UGV [WWW] http://www.philsalesses.com/vegetation-classification-ugv/ (25.05.2013)

16.   Pioneer 3-AT [WWW] http://www.mobilerobots.com/researchrobots/p3at.aspx (29.05.2013)

17.   Seekur Jr [WWW] http://www.mobilerobots.com/researchrobots/SeekurJr.aspx (29.05.2013)

18.   Gas-Powered Mobile Robot [WWW] http://websrv.mece.ualberta.ca/intranet/public.php/research_inventory/display_research_inventory/id/724 (25.05.2013)

19.   Universal Ground Vehicle, Research project L523, 2005-2008

20.   Jitendra R. Raol. Robotic and Moving Vehicle Architectures. /eds. J. R. Raol & A. K. Gopal, ― *Mobile Intelligent Autonomous Systems* 259–269

21.   Mtshali, M., Engelbrecht, A. Robotic Architectures. ― *Defence Science Journal*. 2010, 60(1), 15–22

22.   Shieh, R., Lu, Y. Jerk-Constrained Time-Optimal Control of a Positioning Servo. ― *International Conference on Control Automation and Systems 2010, ICCAS*. 2010, 1473–1476

23.   Minimization, J. Motion Trajectory Planning of Space Manipulator for Joint. ― *International Conference on Mechatronics and Automation 2007, ICMA*. 2007, 3543–3548

24.   Li, H. Z., Gong, Z., Lin, W., Lippa, T. A New Motion Control Approach for Jerk and Transient Vibration Suppression. ― *IEEE International Conference on Industrial Informatics 2006*. Singapore, 2006, 00 676–681

25.   Veeraklaew, T., Piromsopa, P., Chirungsarpsook, K., Pattaravarangkur, C. A Study on the Comparison between Minimum Jerk and Minimum Energy of Dynamic Systems. ― *International Conference on Computational Intelligence for Modelling, Control and Automation and International Conference on Intelligent Agents, Web Technologies and Internet Commerce, CIMCA-IAWTIC'06*. IEEE, 2005, 1 523–528

26.   Johnson, J. a., Neubert, J. Robotic reactive motion with jerk reduction. ― *IEEE International Conference on Robotics and Biomimetics 2012 , ROBIO*. IEEE, 2012, 1421–1426

27.   Zhanli, Z., Shijun, G. A New Acceleration and Deceleration Algorithm and Applications. ― *International Conference on Intelligent Systems Design and Engineering 2012*. Sanya, 2012, 121–124

28.   Shi, X., Xu, B., Xie, W., Li, B. Design and implementation of s-shape acceleration/deceleration algorithm based on rounding error compensation tactic. ― *7th World Congress on Intelligent Control and Automation 2008, WCICA 2008*. 2008, 7912–7916

29.   Rew, K.-H., Kim, K.-S. A complete solution to asymmetric S-curve motion profile: Theory & experiments. ― *International Conference on Control, Automation and Systems 2008*. Seoul: IEEE, 2008, 2845–2849

30.   Le, M. D., Gong, Z. M., Lin, W. Motion Profile Design to Reduce Residual Vibration of High-Speed Positioning Stages. ― *IEEE/ASME Transactions on Mechatronics*. 2009, 14(2), 264–269

31.   Yu, H., Gong, J., Iagnemma, K., Jiang, Y., Duan, J. Robotic wheeled vehicle ripple tentacles motion planning method. ― *IEEE Intelligent Vehicles Symposium 2012*. IEEE, 2012, 1156–1161

32.   Lavalle, S. M. Introduction. ― *Planning Algorithms*. Cambridge University Press, 2006,

33.   Ke-ke, W., Han-qing, Z. A motion planning algorithm for autonomous land vehicle based on virtual tentacles. ― *Control and Decision Conference, CCDC*. 2011, 2431–2435

34.   Cherubini, A., Spindler, F., Chaumette, F. A new tentacles-based technique for avoiding obstacles during visual navigation. ― *IEEE International Conference on Robotics and Automation 2012*. IEEE, 2012, 4850–4855

35. Kneževiü, B., Blanusa, B., Marcetic, D. Model of Elevator Drive With Jerk Control. — *XXIII International Symposium on Information, Communication and Automation Technologies 2011, ICAT*. Sarajevo, 2011, (1), 1–5

36. Martinez, J.-J., Canudas-de-Wit, C. A Safe Longitudinal Control for Adaptive Cruise Control and Stop-and-Go Scenarios. — *IEEE Transactions on Control Systems Technology*. 2007, 15(2), 246–258

37. Yoong, M., Gan, Y., Gan, G. Studies of Regenerative Braking in Electric Vehicle. — *IEEE Conference on Sustainable Utilization and Development in Engineering and Technology 2010, STUDENT*. 2010, (11), 40–45

38. Martinez, J. L. Approximating Kinematics for Tracked Mobile Robots. — *The International Journal of Robotics Research*. 2005, 24(10), 867–878

39. Campa, G. Multitrack 3D Simulink Scope 3DScope. Matlab Central, 2005,

40. Abbadi, A., Matousek, R. RRTs Review and Statistical Analysis. — *International Journal of Mathematics and Computers in Simulation*. 2012, 6(1), 1–8

41. Hachour, O. The Proposed Hybrid Intelligent System for Path Planning of Intelligent Autonomous Systems. — *International Journal of Mathematics and Computers in Simulation*. 2009, 3(3), 133–145

42. Hudjakov, R. *Long-Range Navigation for Unmanned Off-Road Ground Vehicle*. Tallinn University of Technology, 2012,

43. Rohde, M., Perlin, V. PointCom: Semi-autonomous UGV Control With Intuitive Interface. — *SPIE Proceedings 6962, Unmanned Systems Technology X*. web.mit.edu, 2010, 6962

OTHER PUBLICATIONS

1. Hiiemaa, M., Tamre, M. Low Speed Motion Feedback from the Unmanned Ground Vehicle Wheels by Single-Pole Magnetic Encoders. /ed. R. Lahtmets, ― *Proc of 12th International Symp Topical Problems in the Field of Electrical and Power Engineering.* 2012, 145–146

2. Hiiemaa, M., Tamre, M. Using Wireless Sensor Network Components in Practical Assignments of Master's Study Mechatronics Course. ― *10th International Symp Topical Problems in the Field of Electrical and Power Engineering.* Pärnu : Estonian Society of Moritz Hermann Jacobi, 2011, 9234 193–196

3. Hiiemaa, M., Tamre, M. Practical Issues in Utilizing Intelligent Motion Control Layer in UGV-type Robots. ― *8th International Symp. Topical Problems in the Field of Electrical and Power Engineering.* Tallinn : Tallinn University of Technology, 2010, 190–192

4. Hiiemaa, M., Tamre, M. Reconfigurable Battery Pack for Unmanned Ground Vehicle. ― *Proc. of 9th International Symposium „Topical Problems in the Field of Electrical and Power Engineering.* Tallinn : Estonian Society of Moritz Hermann Jacobi, 2010, 200–203

5. Hiiemaa, M., Tamre, M. UGV-type robot motion simulation. ― *7th Int. Symp. Topical Problems in the Field of Electrical and Power Engineering.* Tallinn : Estonian Society of Moritz Hermann Jacobi, 2009, 43–46

6. Sell, R., Hellgren, M., Kask, A., Koch, A., Hiiemaa, M., Seiler, S. Hands-On Lab Exercises. /eds. M. Hellgren & R. Sell, ― *Integrated Systems & Design.* Vilnius : Vilnius Pedagogical University, 2008.

7. Sell, R., Tamre, M., Hiiemaa, M., Leitaru, E., Salong, P. Hybrid Locomotion of Autonomous Vehicle - UGV. ― *8th International Workshop on Research and Education in Mechatronics.* Tallinn : TUT Press, 2007, 305–311

8. Sternfeld, R., Hiiemaa, M., Sell, R., Leomar, P., Tamre, M. Design of a Module-Architectured Autonomous Robot Platform Indigo. Stockholm : KTH - the Royal Institute of Technology, 2005, 1–8

ACKNOWLEDGEMENTS

Foremost, I would like to express my gratitude to my supervisor Prof. Mart Tamre for his continuous support during my PhD study and research, for his patience, enthusiasm, and useful advice. I could not have had a better advisor and mentor for my PhD study.

Besides my supervisor, I would like to thank the rest of my thesis committee for their insightful comments and questions.

My sincere thanks also go to my former UGV development team-mates and current collegues in TUT for especially warm and supportive work environment.

I would also like to thank my wife Kersti and my children Reimo and Keitlin for being patient with me, as I was not available for them as much as they would have liked during my work with the thesis.

ABSTRACT

4-wheel skid-steer Unmanned Ground Vehicles (UGVs) have a simple design. Still, their excellent maneuverability in tight spaces and relatively low cost make them suitable for a variety of applications. Many mobile robots with low center of mass do not necessarily require the use of sophisticated motion planning algorithms, but could benefit from the energy efficient low impact on the UGV system and loading. Robots with high center of mass tend to rock when deceleration is too intense. Impact reduction on the UGV system and safety-critical loading and keeping critical motion parameters limited while allowing maximum controllability by the user input are the problems in focus. Solving these problems with the methods which can be used in UGV control and providing models for testing the efficiency of proposed concepts are the main objectives of the thesis.

Review of the literature is given in Chapter 1. Straight driving mode on a horizontal flat terrain is discussed in Chapter 2. Chapter 3 analyzes a possibility to use AMPP (Active Motion Profile Planner) modules for controlling tangential motion of the left and right side reference point of the UGV. Chapter 4 provides a solution for keeping the maximum acceleration magnitude within safe limits. In Chapter 5 the proposed methods are evaluated to be used in UGV trajectory planning.

This thesis proposes an AMPP for controlling tangential motion of the left and right side reference points. AMPP modules use feedback from the UGV motion and the limits of tangential jerk, tangential acceleration and tangential velocity limit for creating safe and suitable motion profiles one time-step at a time. AMPP modules prevent collisions and parameter overshoots by making short motion simulations every time-step and actively adjusting the planned motion scenarios based on the most recent data when needed.

Low jerk motion has been proven to reduce the wear of actuator systems. It has been reported to reduce residual vibrations as well. Such improvements are desirable for robots of almost any application. For example, the UGV developed and built in TUT Department of Mechatronics (in 2008) has a capability to increase its clearance and center of weight and may become particularly sensitive to sudden mechanical excitations by the wheel servos. Limited and shaped jerk helps to prevent unwanted rocking of the vehicle (on inflated tires and torsion springs of its legs) when the UGV is accelerated or decelerated. UGV undercarriages without suspension would propagate high jerk and acceleration pulses into the UGV frame. More specific applications of UGVs may require safety-critical loading. Removal of IEDs (Improvised Explosive Devices), surveillance with high antenna or microphone matrixes or even the transportation of personnel requires even more motion parameters to be kept within their prescribed limits. Even on flat terrain, human errors of unprocessed manual control of a skid-steer vehicle may cause too high levels of jerk or acceleration within the Critical Area of the UGV and inflict damage to the instrumentation.

Merging of centripetal acceleration vector field and tangential acceleration vector fields was investigated to find the criteria for keeping the magnitude of the maximum lateral acceleration within the Critical Area within prescribed limits. Developed Command Pre-Processor (CPP) that contains control modules for input command processing adds a capability to keep acceleration in any part of the UGV Critical Area within safe levels by the exclusion of unsafe velocity combinations from the input command space. Proportional Velocity Command Reduction (PVCR) module was added to the CPP to exclude unsafe velocity combinations and to reduce the velocity of the left and right side reference points while maintaining the original turning radius. STRA (Small Turning Radius Avoidance) module eliminated the acceleration magnitude violation exception when the UGV spiraled out of the zero-radius turn. It was shown that certain small radius turns are unnecessary for UGV control except zero-radius turning capability, which was not excluded by STRA module. TBB (Turn By Braking) functionality was added to make UGV control more consistent near maximum velocities.

The first main contribution of this thesis is a novel UGV control method for using in skid-steer UGV control to reduce impact on the UGV system and safety-critical loading. The second main contribution is a method of using novel AMPP and a CPP for the skid-steer UGV control keeping critical motion parameters within their limits while allowing maximum controllability by the user input. Thirdly, virtual models which were developed proved the proposed concepts to be effective in skid-steer UGV control.

Analyses of the proposed control concepts suggest the possibility to use them also for semi- and full autonomous control of skid-steer UGVs in future research.

KOKKUVÕTE

Neljarattalistel külisroolimisega mehitamata maasõidukite (UGV-de) konstruktsioon on lihtne, aga nende suurepärane manööverdamisvõime ja suhteliselt madal hind muudavad nende kasutamise väga paljudes rakendustes sobivaks. Paljud madala massikeskmega mobiilsed robotid ei vaja ilmtingimata keerulisi liikumist planeerivaid algoritme, kuid liikumisprofiilide plaanija abil saaks suurendada nende energiatõhusust ning vähendada lööke UGV süsteemile ja kandamile.

Kõrge massikeskmega maasõidukid kipuvad intensiivse pidurdamise korral õõtsuma. Löökide vähendamine UGV süsteemile ja kandamile ja kriitiliste liikumisparameetrite piiramine, samal ajal kui tagatakse UGV maksimaalne juhitavus, on põhilised probleemid, millele töös keskendutakse. Töö peamisteks eesmärkideks on meetodite väljatöötamine, mis taolised probleemid lahendaks, ja mudelite väljatöötamine, mis võimaldaks väljapakutud meetodite tõhusust testida.

Esimeses peatükis antakse kirjanduse ülevaade. Teises peatükis käsitletakse otseliikumist tasasel horisontaalsel maastikul. Kolmandas peatükis analüüsitakse võimalust kasutada UGV juhtimiseks kahte AMPP (Active Motion Profile Planner) moodulit. Peatükis 4 pakutakse välja lahendus, kuidas piirata kriitilises alas (CA) maksimaalse kiirenduse magnituudi. Peatükis 5 hinnatakse väljapakutud meetodite kasutamisvõimalusi UGV trajektoori plaanimisel.

See väitekiri pakub välja UGV vasaku ja parema tugipunkti juhtimiseks aktiivse liikumisprofiili plaanija (AMPP). AMPP moodulid kasutavad ohutute ja sobivate liikumisprofiilide, ühe ajasammu kaupa moodustamiseks, liikumise tagasisidet ja tangensiaalse tõuke, kiirenduse ja kiiruse piiranguid. AMPP moodulid ennetavad kokkupõrkeid ja etteantud liikumisparameetrite ületamisi selliselt, et teevad igal ajasammul lähtuvalt kõige värskematest lähteandmetest lühikesi liikumise simulatsioone ja muudavad plaanitavaid liikumisstsenaariume vastavalt vajadusele.

Madala tõuketasemega liikumine vähendab täiturmehhanismide kulumist ja jääkvõnkumisi. Näiteks võib tuua UGV, mis arendati välja ja valmistati TTÜ mehhatroonikainstituudis (2008. a). Sellel on võime muuta oma kliirensit ja raskuskeset ning seeläbi võib muutuda ratta servode järskudele liikumistele eriliselt tundlikuks. Piiratud ja modifitseeritud tõukeprofiil aitab ära hoida sõiduki kiirendamisel ja aeglustamisel tekkida võivat õõtsumist (õhkrehvidel ja torsioonvedrustusel). Ilma vedrustuseta UGV veermikud edastaksid tugevad tõuke ja kiirenduse impulsid UGV raami ja kandamini. Spetsiifilisemad UGV rakendused võivad nõuda tundlikku kandamit, mis peab olema selliste impulsside eest kaitstud. Improviseeritud lõhkeseadeldiste teisaldamine ning kõrgete antennisüsteemidega või mikrofonimaatriksitega seire vajavad täiendavaid liikumisparameetrite piiranguid. Kui kasutada UGV juhtimiseks töötlemata sisendeid, võib inimliku vea tõttu isegi tasasel maastikul sõites tekkida UGV raamis tõuke või kiirenduse tase, mis rikub kandamit.

Maksimaalse külgsuunalise kiirenduse magnituudi piiramiseks uuriti UGV raamis tangensiaalkiirenduse ja kesktõmbekiirenduse vektorväljade liitumist.

Väljaarendatud juhtkäskude eeltöötlemise moodul (CPP) võimaldab ohtlike kiirusekombinatsioonide käsuruumist eemaldamise abil maksimaalset kiirenduse magnituudi vajaliku tasemeni piirata. Selleks, et UGV kiirust vähendada, jättes algselt valitud pöörderaadius muutmata, lisati CPP-le kiirusekäskude proportsionaalse vähendamise moodul (PVCR), mis vähendab UGV vasaku ja parema poole tugipunkti kiirust võrdeliselt. Väikese pöörderaadiuse vältimise moodul (STRA) lubab kasutada kohapealpööramist, kuid kaotab ebapraktiliselt väikeste pöörderaadiuste kasutamise võimaluse. Sellega välistatakse erandliku situatsiooni tekkimine, kus UGV ületab kiirenduse magnituudi piirangut, minnes kohapealpööramiselt vahetult üle otseliikumisele. Töös näidati, et välistatud pöörderaadiused olid UGV juhtimise seisukohast ebaolulised. Pidurdamisel pööramise (TBB) funktsionaalsus lisati selleks, et UGV juhtimine oleks ka vasaku ja parema poole maksimumkiiruste juures ühesugune.

Töö esimeseks peamiseks panuseks on uudse meetodi väljatöötamine, mida saab kasutada külisroolimisega UGV juhtimiseks, et vähendada lööke UGV süsteemile ja kandamile. Teine peamine panus on uudse AMPP ja CPP kasutamise meetod UGV juhtimises, mis võimaldab üheaegselt piirata kriitilisi liikumis-parameetreid ja tagada UGV maksimaalne juhitavus vastavalt kasutajasisendile. Kolmandaks, väljapakutud ideid hinnati Matlabi ja Simulinki abil koostatud mudelite ja simulatsioonide abil. Simulatsioonide tulemused kinnitavad esitatud ideede tõhusust.

Väljapakutud meetodite analüüs lubab ka arvata, et need oleksid kasutatavad ka külisroolimisega mehitamata maasõidukite pool- ja täisautonoomse juhtimise juures edasises teadustöös.

ELULOOKIRJELDUS

1. Isikuandmed
   Ees- ja perekonnanimi   Maido Hiiemaa
   Sünniaeg ja -koht   10.11.1980 Tallinn, Eesti Vabariik
   Kodakondsus   Eesti

2. Kontaktandmed
   Aadress   Orava 7, Tallinn 11214
   Telefon   53 909 109
   E-posti aadress   maido.hiiemaa@ttu.ee

3. Hariduskäik

Õppeasutus (nimetus lõpetamise ajal)	Lõpetamise aeg	Haridus (eriala/kraad)
Tallinna Tehnikaülikool	2006	Arvuti- ja süsteemitehnika eriala (Dipl. -Ing)
Tallinna Tehnikaülikool	2003	Arvutisüsteemide eriala (M.Sc.)
Tallinna Tehnikagümnaasium	1999	(keskharidus)

4. Keelteoskus (alg-, kesk- või kõrgtase)

Keel	Tase
Eesti keel	kõrgtase
Inglise keel	kõrgtase
Soome keel	algtase
Vene keel	algtase

5. Teenistuskäik

Töötamise aeg	Tööandja nimetus	Ametikoht
2007 - ...	Tallinna Tehnikaülikool, Mehhatroonikainstituut	teadur
2004 - 2006	Tallinna Tehnikaülikool, Mehhatroonikainstituut	insener

6. Kaitstud lõputööd

Magistritöö: Servo liidesed FPGA-l, 2006, juhendaja Peeter Ellervee, Tallinna Tehnikaülikool

Diplomitöö: MIDI Klaviatuurikontroller, juhendaja Arvo Toomsalu, 2003, Tallinna Tehnikaülikool

7. Teadustöö põhisuunad

- Mehitamata maasõiduki (UGV) elektroonika ja juhtimine
- Reaalajasüsteemid
- Riistvara disain ja programmeerimine

CURRICULUM VITAE

1. Personal data

Name	Maido Hiiemaa
Date and place of birth	10.11.1980, Tallinn Estonia

2. Contact information

Address	Orava 7, Tallinn 11214
Phone	(+372) 53 909 109
E-mail	maido.hiiemaa@ttu.ee

3. Education

Educational institution	Graduation year	Education (field of study/degree)
Tallinn University of Technology	2006	Computer and Systems Engineering (Dipl. -Ing)
Tallinn University of Technology	2003	Computer Systems, diploma study (M.Sc.)
Tallinn High school of Technology	1999	(High school education)

4. Language competence/skills (fluent; average, basic skills)

Language	Level
Estonian	fluent
English	fluent
Finnish	basic skills
Russian	basic skills

5. Professional Employment

Period	Organization	Position
2007 - present	Tallinn Univ. of Technology, Dept. of Mechatronics	researcher
2004 - 2006	Tallinn Univ. of Technology, Dept. of Mechatronics	engineer

6. Defended theses

Master's thesis: Servo interfaces on FPGA, 2006, supervisor Peeter Ellervee, Tallinn University of Technology

Diploma thesis: MIDI Keyboard Controller, supervisor Arvo Toomsalu, 2003, Tallinn University of Technology

7. Main areas of scientific work/Current research topics

- Electronics and control of skid-steer UGVs
- Real-time systems
- Hardware design and programming

DISSERTATIONS DEFENDED AT
TALLINN UNIVERSITY OF TECHNOLOGY ON
MECHANICAL ENGINEERING

1. **Jakob Kübarsepp**. Steel-Bonded Hardmetals. 1992.

2. **Jakub Kõo**. Determination of Residual Stresses in Coatings &Coated Parts. 1994.

3. **Mart Tamre**. Tribocharacteristics of Journal Bearings Unlocated Axis. 1995.

4. **Paul Kallas**. Abrasive Erosion of Powder Materials. 1996.

5. **Jüri Pirso**. Titanium and Chromium Carbide Based Cermets. 1996.

6. **Heinrich Reshetnyak**. Hard Metals Serviceability in Sheet Metal Forming Operations. 1996.

7. **Arvi Kruusing**. Magnetic Microdevices and Their Fabrication methods. 1997.

8. **Roberto Carmona Davila**. Some Contributions to the Quality Control in Motor Car Industry. 1999.

9. **Harri Annuka**. Characterization and Application of TiC-Based Iron Alloys Bonded Cermets. 1999.

10. **Irina Hussainova**. Investigation of Particle-Wall Collision and Erosion Prediction. 1999.

11. **Edi Kulderknup**. Reliability and Uncertainty of Quality Measurement. 2000.

12. **Vitali Podgurski**. Laser Ablation and Thermal Evaporation of Thin Films and Structures. 2001.

13. **Igor Penkov**. Strength Investigation of Threaded Joints Under Static and Dynamic Loading. 2001.

14. **Martin Eerme**. Structural Modelling of Engineering Products and Realisation of Computer-Based Environment for Product Development. 2001.

15. **Toivo Tähemaa**. Assurance of Synergy and Competitive Dependability at Non-Safety-Critical Mechatronics Systems design. 2002.

16. **Jüri Resev**. Virtual Differential as Torque Distribution Control Unit in Automotive Propulsion Systems. 2002.

17. **Toomas Pihl**. Powder Coatings for Abrasive Wear. 2002.

18. **Sergei Letunovitš**. Tribology of Fine-Grained Cermets. 2003.

19. **Tatyana Karaulova**. Development of the Modelling Tool for the Analysis of the Production Process and its Entities for the SME. 2004.

20. **Grigori Nekrassov**. Development of an Intelligent Integrated Environment for Computer. 2004.

21. **Sergei Zimakov**. Novel Wear Resistant WC-Based Thermal Sprayed Coatings. 2004.

22. **Irina Preis**. Fatigue Performance and Mechanical Reliability of Cemented Carbides. 2004.

23. **Medhat Hussainov**. Effect of Solid Particles on Turbulence of Gas in Two-Phase Flows. 2005.

24. **Frid Kaljas**. Synergy-Based Approach to Design of the Interdisciplinary Systems. 2005.

25. **Dmitri Neshumayev**. Experimental and Numerical Investigation of Combined Heat Transfer Enhancement Technique in Gas-Heated Channels. 2005.

26. **Renno Veinthal**. Characterization and Modelling of Erosion Wear of Powder Composite Materials and Coatings. 2005.

27. **Sergei Tisler**. Deposition of Solid Particles from Aerosol Flow in Laminar Flat-Plate Boundary Layer. 2006.

28. **Tauno Otto**. Models for Monitoring of Technological Processes and Production Systems. 2006.

29. **Maksim Antonov**. Assessment of Cermets Performance in Aggressive Media. 2006.

30. **Tatjana Barashkova**. Research of the Effect of Correlation at the Measurement of Alternating Voltage. 2006.

31. **Jaan Kers**. Recycling of Composite Plastics. 2006.

32. **Raivo Sell**. Model Based Mechatronic Systems Modeling Methodology in Conceptual Design Stage. 2007.

33. **Hans Rämmal**. Experimental Methods for Sound Propagation Studies in Automotive Duct Systems. 2007.

34. **Meelis Pohlak**. Rapid Prototyping of Sheet Metal Components with Incremental Sheet Forming Technology. 2007.

35. **Priidu Peetsalu**. Microstructural Aspects of Thermal Sprayed WC-Co Coatings and Ni-Cr Coated Steels. 2007.

36. **Lauri Kollo**. Sinter/HIP Technology of TiC-Based Cermets. 2007.

37. **Andrei Dedov**. Assessment of Metal Condition and Remaining Life of In-service Power Plant Components Operating at High Temperature. 2007.

38. **Fjodor Sergejev**. Investigation of the Fatigue Mechanics Aspects of PM Hardmetals and Cermets. 2007.

39. **Eduard Ševtšenko**. Intelligent Decision Support System for the Network of Collaborative SME-s. 2007.

40. **Rünno Lumiste**. Networks and Innovation in Machinery and Electronics Industry and Enterprises (Estonian Case Studies). 2008.

41. **Kristo Karjust**. Integrated Product Development and Production Technology of Large Composite Plastic Products. 2008.

42. **Mart Saarna**. Fatigue Characteristics of PM Steels. 2008.

43. **Eduard Kimmari**. Exothermically Synthesized B_4C-Al Composites for Dry Sliding. 2008.

44. **Indrek Abiline**. Calibration Methods of Coating Thickness Gauges. 2008.

45. **Tiit Hindreus**. Synergy-Based Approach to Quality Assurance. 2009.

46. **Karl Raba**. Uncertainty Focused Product Improvement Models. 2009.

47. **Riho Tarbe**. Abrasive Impact Wear: Tester, Wear and Grindability Studies. 2009.

48. **Kristjan Juhani**. Reactive Sintered Chromium and Titanium Carbide-Based Cermets. 2009.

49. **Nadežda Dementjeva**. Energy Planning Model Analysis and Their Adaptability for Estonian Energy Sector. 2009.

50. **Igor Krupenski**. Numerical Simulation of Two-Phase Turbulent Flows in Ash Circulating Fluidized Bed. 2010.

51. **Aleksandr Hlebnikov**. The Analysis of Efficiency and Optimization of District Heating Networks in Estonia. 2010.

52. **Andres Petritšenko**. Vibration of Ladder Frames. 2010.

53. **Renee Joost**. Novel Methods for Hardmetal Production and Recycling. 2010.

54. **Andre Gregor**. Hard PVD Coatings for Tooling. 2010.

55. **Tõnu Roosaar**. Wear Performance of WC- and TiC-Based Ceramic-Metallic Composites. 2010.

56. **Alina Sivitski**. Sliding Wear of PVD Hard Coatings: Fatigue and Measurement Aspects. 2010.

57. **Sergei Kramanenko**. Fractal Approach for Multiple Project Management in Manufacturing Enterprises. 2010.

58. **Eduard Latõsov**. Model for the Analysis of Combined Heat and Power Production. 2011.

59. **Jürgen Riim**. Calibration Methods of Coating Thickness Standards. 2011.

60. **Andrei Surzhenkov**. Duplex Treatment of Steel Surface. 2011.

61. **Steffen Dahms**. Diffusion Welding of Different Materials. 2011.

62. **Birthe Matsi**. Research of Innovation Capasity Monitoring Methodology for Engineering Industry. 2011.

63. **Peeter Ross**. Data Sharing and Shared Workflow in Medical Imaging. 2011.

64. **Siim Link**. Reactivity of Woody and Herbaceous Biomass Chars. 2011.

65. **Kristjan Plamus**. The Impact of Oil Shale Calorific Value on CFB Boiler Thermal Efficiency and Environment. 2012.

66. **Aleksei Tšinjan**. Performance of Tool Materials in Blanking. 2012.

67. **Martinš Sarkans**. Synergy Deployment at Early Evaluation of Modularity of the Multi-Agent Production Systems. 2012.

68. **Sven Seiler**. Laboratory as a Service – A Holistic Framework for Remote and Virtual Labs. 2012.

69. **Tarmo Velsker**. Design Optimization of Steel and Glass Structures. 2012.

70. **Madis Tiik**. Access Rights and Organizational Management in Implementation of Estonian Electronic Health Record System. 2012.

71. **Marina Kostina**. Reliability Management of Manufacturing Processes in Machinery Enterprises. 2012.

72. **Robert Hudjakov**. Long-Range Navigation for Unmanned Off-Road Ground Vehicle. 2012.

73. **Arkadi Zikin**. Advanced Multiphase Tribo-Functional PTA Hardfacings. 2013.

74. **Alar Konist**. Environmental Aspects of Oil Shale Power Production. 2013.

75. **Inge Roos**. Methodology for Calculating CO_2 Emissions from Estonian Shale Oil Industry. 2013.

76. **Dmitri Shvarts**. Global 3D Map Merging Methods for Robot Navigation. 2013.

77. **Kaia Lõun**. Company's Strategy Based Formation of e-Workplace Performance in the Engineering Industry. 2013.